Evidence of Early Holocene outburst floods from landslide-dammed lakes in the Central Baikal Rift Zone, Eastern Siberia

S.G. Arzhannikov, A.V. Arzhannikova, Regis Braucher, A.A. Chebotarev

Quaternary International 763 (2026) 110198

Contents lists available at ScienceDirect

Quaternary International

journal homepage: www.elsevier.com/locate/quaint

Evidence of Early Holocene outburst floods from landslide-dammed lakes in the Central Baikal Rift Zone, Eastern Siberia

S.G. Arzhannikov [a,*], A.V. Arzhannikova [a], R. Braucher [b], A.A. Chebotarev [a]

[a] Institute of the Earth's Crust, Russian Academy of Sciences, Siberian Branch, Lermontova str., 128, 664033, Irkutsk, Russia
[b] CEREGE, CNRS-IRD-Collège de France-INRAE, Aix-Marseille Univ., 13545, Aix-en-Provence, France

ARTICLE INFO

Keywords:
Landslide dammed-lake
Outburst flood sediment
Seismogenic fault
Remote sensing and mapping
^{10}Be
^{26}Al cosmic-ray exposure dating
OSL dating
Baikal Rift Zone

ABSTRACT

Landslide-dammed lake outburst floods represent a significant hazard and are a major focus of natural risk assessment. Despite the extensive documentation of such events globally, comprehensive research on outburst floods from dammed lakes in southern East Siberia remains insufficient. A striking example of this understudied phenomenon is the unique Ina Rock Garden, located in the Barguzin Basin (Baikal Rift Zone). The aim of this research is to determine the genesis of this landscape and to reconstruct the parameters, conditions, and age of the catastrophic event. For the first time in the central part of the Baikal Rift Zone, a comprehensive paleogeographic reconstruction of a catastrophic landslide-dammed lake outburst has been conducted, establishing its morphology, chronology, hydraulic parameters, and link to seismotectonic activity. Remote sensing data analysis revealed a series of landslides, two of which functioned as dams. We propose that the formation and subsequent breaching of the dams resulted from earthquakes of M = 7–8 associated with the Barguzin and Ukshum fault zones. Evidence of these earthquakes is preserved in the topography as a series of seismogenic scarps. The breach of the landslide dam led to intense erosion and subsequent accumulation of various types and sizes of deposits, situated at different topographic levels within the Ina River valley. The flow depth exceeded 50 m. Sedimentation and subsequent erosion formed bars, terraces and an alluvial fan. The distribution of boulder deposits along the Ina River valley is uneven and has a patchy pattern: areas of boulder concentration alternate with zones dominated by sand and gravel deposits. This indicates significant variations in flow dynamics associated with the widening and narrowing of the river valley. The calculated peak discharge of the flood ranges from 64,000 to 131,900 m^3/s, which is comparable to major 20th-century events, such as the Yigong outburst flood in Tibet in 2000. Cosmogenic dating (^{10}Be, ^{26}Al) of boulders from the alluvial fan and OSL-dating of sand and gravel deposits from the terrace constrain the outburst flood between 9.1 ka and 10.7 ka. This period correlates with a strong paleo-earthquake in the Barguzin fault zone (M = 7.5–8.0), indicating a seismic trigger for both the formation of the landslide dams and, likely, their subsequent failure. The obtained results are of fundamental importance for understanding the role of dammed-lake outburst floods in the landscape formation and represent a significant contribution to the assessment of modern natural hazards.

1. Introduction

Outburst floods as a natural disaster were first described in the Middle Ages (Carozzi and Carozzi, 1987); however, a detailed and systematic study of lake drainage floods began only in the 20th century. The founders of the megaflood hypothesis were American researchers G. K. Gilbert, J.H. Bretz, and J.T. Pardee (Gilbert, 1890; Pardee, 1910, 1942; Bretz, 1928; Bretz et al., 1956). These discoveries initiated research into the erosional activity of cataclysmic floods and their role in shaping unique landscapes (Pardee, 1942; Bretz et al., 1956; Carling, 2013; Baker, 2020; Bjornstad, 2021). Studies of this phenomenon (Baker, 2009, 2020) have found numerous evidence of outburst floods in North America (O'Connor, 1993; Clarke et al., 2004; Carter et al., 2006; Clayton and Knox, 2008; Wiedmer et al., 2010; Breckenridge, 2015; Waitt, 2016; Fisher, 2020), South America (Benitoa and Thorndycraft, 2020), and Europe (Russell et al., 2005; Meinsen et al., 2011; Komatsu et al., 2016; Høgaas and Longva, 2016; Lang et al., 2019; Carrivick and Tweed, 2019). For Northern Asia, the issue of megafloods has been considered in connection with the outburst of periglacial lakes in Tibet (Montgomery et al., 2004; Huang et al., 2014, 2024; Hu et al., 2018),

* Corresponding author.
E-mail addresses: sarzhan@crust.irk.ru (S.G. Arzhannikov), braucher@cerege.fr (R. Braucher).

https://doi.org/10.1016/j.quaint.2026.110198
Received 5 May 2025; Received in revised form 22 February 2026; Accepted 24 February 2026
Available online 5 March 2026

Northern Mongolia (Komatsu et al., 2009, 2016, 2016a, 2016b; Arzhannikov et al., 2023), Altai (Rudoy and Baker, 1993; Carling et al., 2002; Zolnikov and Deev, 2013), and Transbaikalia (Margold et al., 2018; Arzhannikova et al., 2025). Along with the drainage of periglacial lakes, data were obtained on outbursts of Lake Baikal during the formation of new outlets caused by large landslides (Arzhannikov et al., 2018).

Today, there are no giant ice-dammed lakes on the planet capable of causing the kind of catastrophes that occurred during the last Late Pleistocene glaciation and its deglaciation. However, studies of topography in various regions of the world and data from man-made disasters have shown that the formation of outburst flows can be associated with other processes. For example, the collapse of large landslides into man-made reservoirs (Panizzo et al., 2005) and the destruction of constructed and natural dams (Costa, 1985, 1987; Liu et al., 2019) and jökulhlaups (Maizels, 1997; Alho et al., 2005; Russell et al., 2005). To date, extensive statistics have been compiled on disasters associated with the failure of man-made and natural dams (Jansen, 1980; Costa, 1985; Costa and Schuster, 1987; Panizzo et al., 2005; Kaktins et al., 2013; Zhang et al., 2014; Delaney and Evans, 2015; Strom and Abdrakhmatov, 2018; Liu et al., 2019; O'Connor et al., 2022). The main triggers of landslide dam formation are intense precipitation (rain and snowmelt), earthquakes, and human activity. Volcanism can also be a source of landslides, but it accounts for less than 10 percent (Costa and Schuster, 1987).

Landslide-dammed lake outburst floods are common and have been well studied in North America, Central Asia, and Southeast Asia (Costa, 1985; Costa and Schuster, 1987; Delaney and Evans, 2015; Strom and Abdrakhmatov, 2018; Liu et al., 2019). The lifetime of dammed lakes ranges from a few minutes to several thousand years (Costa and Schuster, 1987) and depends on many factors, including the geology of the landslide source area, the type of landslide dam, and the internal structure and grain size of the debris comprising the landslide. The most important characteristic governing dam stability is its resistance to erosion, both on the dam surface from water runoff and inside the dam from seepage. Landslide dams composed of large particles resist failure better than dams containing a large proportion of soil or soft rock (Costa and Schuster, 1987). Because earthquakes play an important role in triggering landslides and dammed lake formation (Adams, 1981; Costa and Schuster, 1987; Evans et al., 2011; Fan et al. 2012a, 2012b; Chen et al., 2013; Xu et al., 2013; Liu et al., 2019), numerous monitoring programs and dedicated studies have been conducted worldwide. For example, the 2008 Wenchuan earthquake in China (M = 8.0), one of the largest earthquakes on record, resulted in widespread landslides and 256 dammed lakes (Cui et al., 2009). This event provided further impetus for more detailed studies of dammed lake outburst hazards (Liu et al., 2019). At the same time, in Siberia, although numerous relict and modern dammed lakes formed as a result of seismogenic collapses and landslides have been documented (Ufimtsev et al., 1998; Arzhannikov, 1998, 2000; Skovitina, 1996, 2002; Komatsu et al., 2009; Arzhannikov et al., 2010; Chebotarev et al., 2024), detailed studies of outburst floods remain fragmentary. To fill this gap, we propose a study of the erosional-accumulative landscape known as the Ina Rock Garden (IRG), which is believed to be the result of catastrophic processes in the Ikatskii Ridge (Ufimtsev et al., 1998). This landscape, comprising erosional scours, boulder bars, and extensive coarse-grained deposits in the Ina River valley, is a diagnostic assemblage of past catastrophic flooding and underscores the necessity for a comprehensive hazard assessment in Siberia (Fig. 1).

On the eastern flank of the Barguzin Basin, where the Ina River emerges from the Ikatskii Ridge, a large alluvial fan composed of blocks up to 9-10 m in size is present (Ufimtsev et al., 2004). This anomalous accumulation of granite blocks attracted the attention of the scientific community and became the subject of geological and geomorphological studies and discussions (Lamakin, 1952; Florensov, 1960; Ufimtsev, 1986). As a result, initial insights were gained about the unique landscape, its morphology and the distribution of coarse clastic deposits in the Ina River valley and in the Barguzin Basin. In the early stages of research, a glacial hypothesis was proposed for the formation of the IRG. The boulder accumulation was interpreted either as a lateral moraine of the Barguzin Glacier, which presumably filled the entire basin (Lamakin, 1952), or as a terminal moraine of the Middle Pleistocene glaciation (Ravskii et al., 1964). A version of a mudflow associated with the outburst of a dammed-lake, presumably located in the Turokcha River valley, was also proposed (Ufimtsev, 1986). However, to date, no consensus has been reached on the cause and timing of this phenomenon, the parameters of the outburst flow, and the extent of its impact on the environment. Initial information on the IRG (Ufimtsev, 1986) indicates a high-energy event capable of transporting a huge amount of large debris and forming a distinctive landscape in the Ina River valley. The extent of the debris distribution and its size indicate the possibility of a past outburst flood, which represents a new type of natural hazard (in addition to high seismic risk) for this region. This highlights the need to address a series of interrelated questions: determining the genetic type of the process that generated the IRG; identifying landforms in the Ina River valley; identifying patterns in the distribution and thickness of sediments; and determining the conditions (flow parameters) and timing of the Ina outburst flood. In this study, we used satellite imagery and digital elevation models (DEMs) to identify areas of landslides and dammed lakes responsible for the formation of the outburst flood. We calculated the parameters of the catastrophic flow, assessed its potential to modify the valley morphology in the outburst flood's impact zone, and, using a comprehensive suite of geochronological methods, determined the timing of its formation.

2. Geographical and geological setting

The study area is located in the central part of the Baikal Rift Zone, which includes the Ikatskii and Barguzin ridges and the Barguzin Basin (Fig. 1a, b, c). The bedrock consists of metamorphic and igneous rocks of Proterozoic and Paleozoic age (Fig. 1b). The river valleys in the Barguzin and Ikatskii ridges have a thin cover of Pleistocene-Holocene sediments. The Barguzin Basin is filled with a Neogene-Quaternary sediment layer over 2000 m thick. The formation of the Barguzin Basin is linked to the geological history of the entire Baikal Rift Zone, the main feature of which is its two-stage development in the Cenozoic: slow and rapid rifting (Logatchev and Zorin, 1987; Mats et al., 2001; Logatchev, 2003; Petit, 2006). The intensification of tectonic processes in the Late Cenozoic is associated with the northward propagation of deformations caused by the Indo-Asian collision (Jolivet et al., 2007).

Today, the Barguzin Basin is an asymmetrical graben striking northeast. The dimensions of the depression are 200 × 35 km. From the west, it is bordered by the Barguzin Ridge (2841 m a.s.l.), from the east – by the Ikatskii Ridge (2573 m a.s.l.). The elevation of the basin floor slowly increases from southwest to northeast from 470 to 600 m a.s.l. The modern landscape of the basin comprises a piedmont plain (colluvium), wide terraces and floodplains, lake-marsh depressions (alluvial deposits) and flat sandy massifs (fluvial deposits) (Fig. 1c). The formation of depressions in the northwestern part of the Barguzin Basin is associated with tectonic subsidence along the Barguzin Fault. The 200-km-long Barguzin Fault consists of three segments: the Ulyun Fault in the southwest, the Saranhur Fault in the center, and the Shaman Fault in the northeast (Fig. 1c). A detailed study of the fault revealed two to four paleoearthquakes with displacement amplitudes of 5–9.5 m, two of which occurred 4500 and 9000 years ago. In total, six earthquakes with magnitudes $7.5 \leq M < 8.0$ and two earthquakes with magnitudes ≥ 8.0 may have occurred in the Barguzin Fault zone over the past 10,000–12,000 years (Chipizubov et al., 2007). On the southeastern side of the Barguzin Basin, where it borders the Ikatskii Ridge, there is no main fault, but there are active faults (Fig. 1c) trending NE-SW and W-E (Lunina and Gladkov, 2007).

The accumulation of large boulders (IRG) discovered in the middle of the 20th century at the mouth of the Ina River (Lamakin, 1952, 1968;

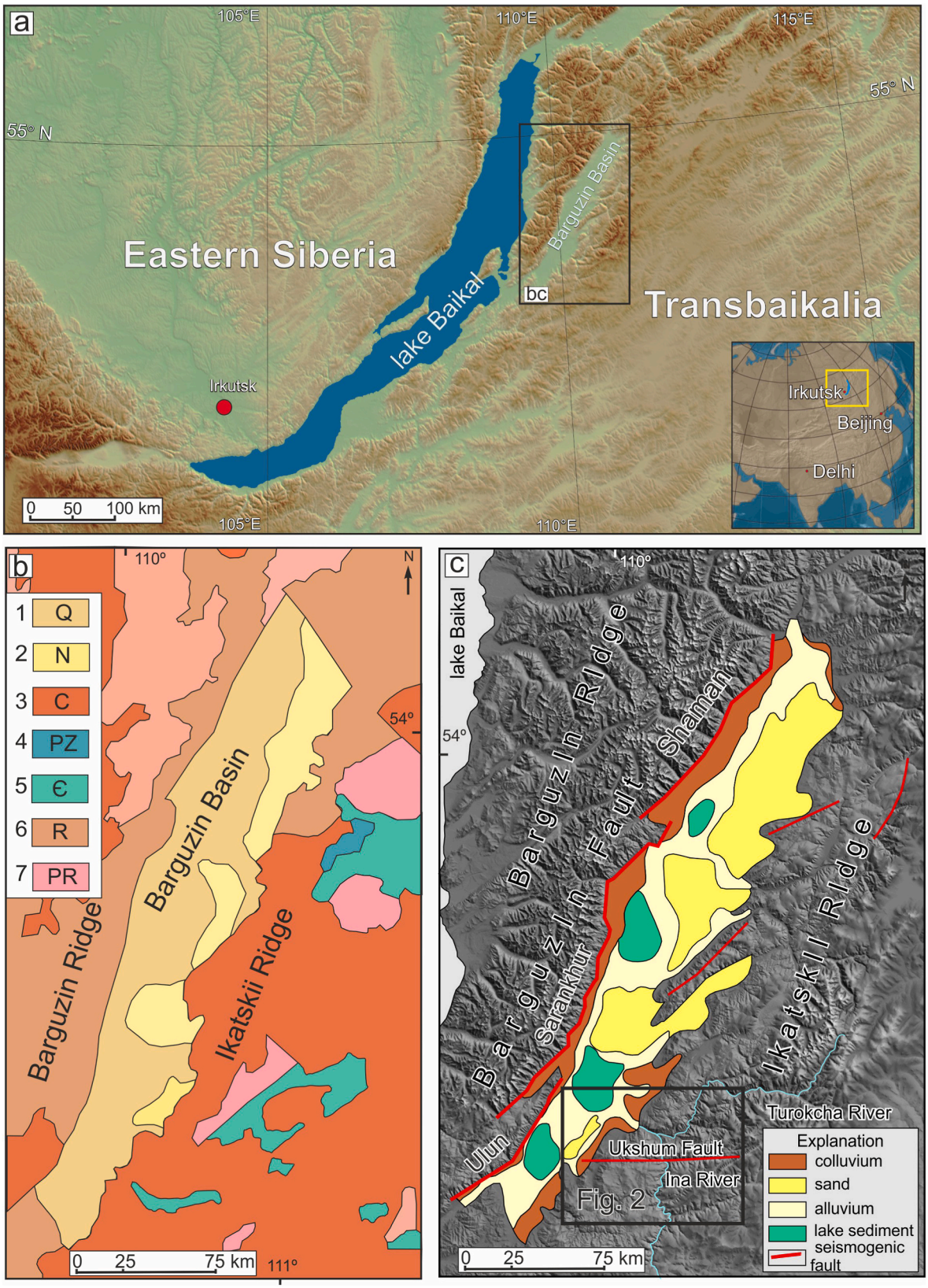

Fig. 1. (a) Location of the Barguzin Basin, Transbaikalia, in the central part of the Baikal rift zone (inset shows location within Asia). (b) Generalized geology of the Barguzin Basin showing the Ikatskii and Barguzin ridges (Hassan, 2022): (1) Quaternary and Neogene: alluvial and eolian sediments. (2) Neogene: alluvial sediments, brown coals. (3) Paleozoic (Carboniferous): granites, syenites, granodiorites. (4) Paleozoic (Ordovician): gabbro, diorites. (5) Cambrian: dolomites, limestones, conglomerates. (6) Proterozoic (Riphean): schists, sandstones, limestones (7) Proterozoic: gneisses, schists. (c) Shaded relief map of the Barguzin Basin, showing seismogenic faults and Quaternary sediments. Black square indicates our study area (see Fig. 2).

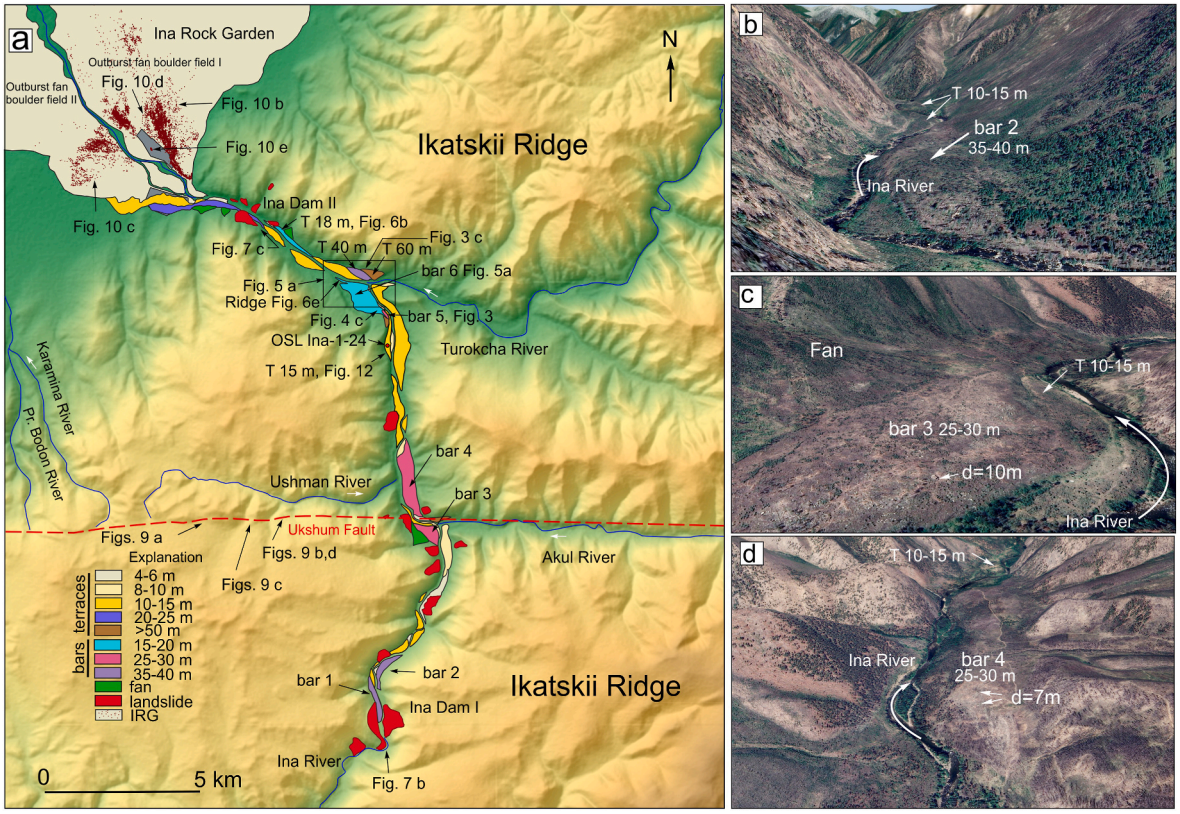

Fig. 2. (a) Study area and observation points of the Ina River valley from Ina Dam I to the Ina Rock Garden, including the location of Fig. 3–12 (base map: SRTM V4 data). Brown dots mark the distribution of boulders within the Ina Rock Garden. (b-d) Satellite images (Google Earth), showing the location and morphology of bars 2-4 and terraces (10-15 m). T – terrace, d – diameter of flood-transported boulder.

Florensov, 1960; Ravskii, 1972) was initially identified as a washed-out moraine. It was only in two papers (Ufimtsev, 1986; Ufimtsev et al., 2004) that this boulder field was interpreted as the result of a catastrophic debris flow or an outburst flood. What did we know about the IRG and outburst topography at the beginning of this study from previous work (Ufimtsev, 1986; Ufimtsev et al., 2004)? IRG and outburst topography are located in the Barguzin Basin and the Ikatskii Ridge (Fig. 2a). They consist of boulder fields, canyons, bedrock and aggradational terraces, hills and ridges composed of unsorted sediments, bedrock ridges, and erratic boulders concentrated in the Ina River valley. The studies by Ufimtsev (1986) and Ufimtsev et al. (2004) present the results of an investigation of a segment of the Ina River valley that extends from its confluence with the Turokcha River to the alluvial fan at its outlet into the Barguzin Basin. These works provide a relatively detailed structural and morphological characterization of the IRG. They document the parameters of individual boulders and their clusters, along with their morphological features. The total area of boulder distribution was determined to be 10 km^2, with boulders penetrating more than 5 km into the central part of the Barguzin Basin. The research also yielded data on the parameters, structure, and topography of the river terraces. TL dates were obtained from terrace deposits (Ufimtsev et al., 2004): 66,000 ± 8000 years for a terrace of 5.5 m (BurGINSORAN, No. 310), 60,000 ± 8000 years for terrace of 14 m (BurGIN SORAN, No. 320), and 71,000 ± 7000 years for terrace of 20 m (BurGIN SORAN, No. 320). These results provided the first chronological data for the terraces in the Ina River valley.

Based on this evidence, the authors concluded that a catastrophic, giant ejection of clastic material occurred from the Ina River valley into the Barguzin Basin. They proposed that this event could have been caused by the drainage of a proglacial lake, a major debris flow, or the outburst of a landslide-dammed lake, with the confluence of the Turokcha River suggested as the most likely damming site (Ufimtsev, 1986). Despite these findings, the ultimate source of the catastrophic influence on the topography of the Ina River valley and the Barguzin Basin remained undetermined. In presenting their conclusions on the IRG, the authors (Ufimtsev et al., 2004) deliberately focused solely on the morphology of this remarkable natural feature, leaving the question of the precise origin of the catastrophic event for future generations of geologists to resolve.

3. Methods and results

3.1. Remote sensing, geomorphic mapping and field surveys

The creation of maps and schemes for the study area was based on the analysis of remote sensing data (including 1-arc-second data from the Shuttle Radar Topography Mission (Farr et al., 2007; http://srtm.csi.cgiar.org) and TanDEM-X (project DEM_Geol 1188; https://tandemx-science.dlr.de) as well as topographic maps, satellite images, and aerial photographs at various scales). The mapping process was as follows. Primary terrain analysis was performed using SRTM data (30 m). TanDEM-X data (12 m) were then used. For more detailed analysis we used satellite images of different resolutions (Google Earth), which were combined with the DEM to obtain a high-quality three-dimensional visualizations. This approach allowed us to analyze the features of the erosional and depositional landscapes in detail. We used geological maps (Gusev and Shobogorov, 1979) to exclude landforms related to lithological features (e.g., contacts of rocks of different compositions). Topographic maps, georeferenced to a single coordinate system, provided information on the toponymy of the main landforms of the study area and served as a basis for correcting the elevation values of digital elevation models (SRTM, TanDEM-X). The main efforts were aimed at searching for geomorphic indicators of catastrophic processes associated with the formation of landslide-dammed and glacier-dammed lakes in

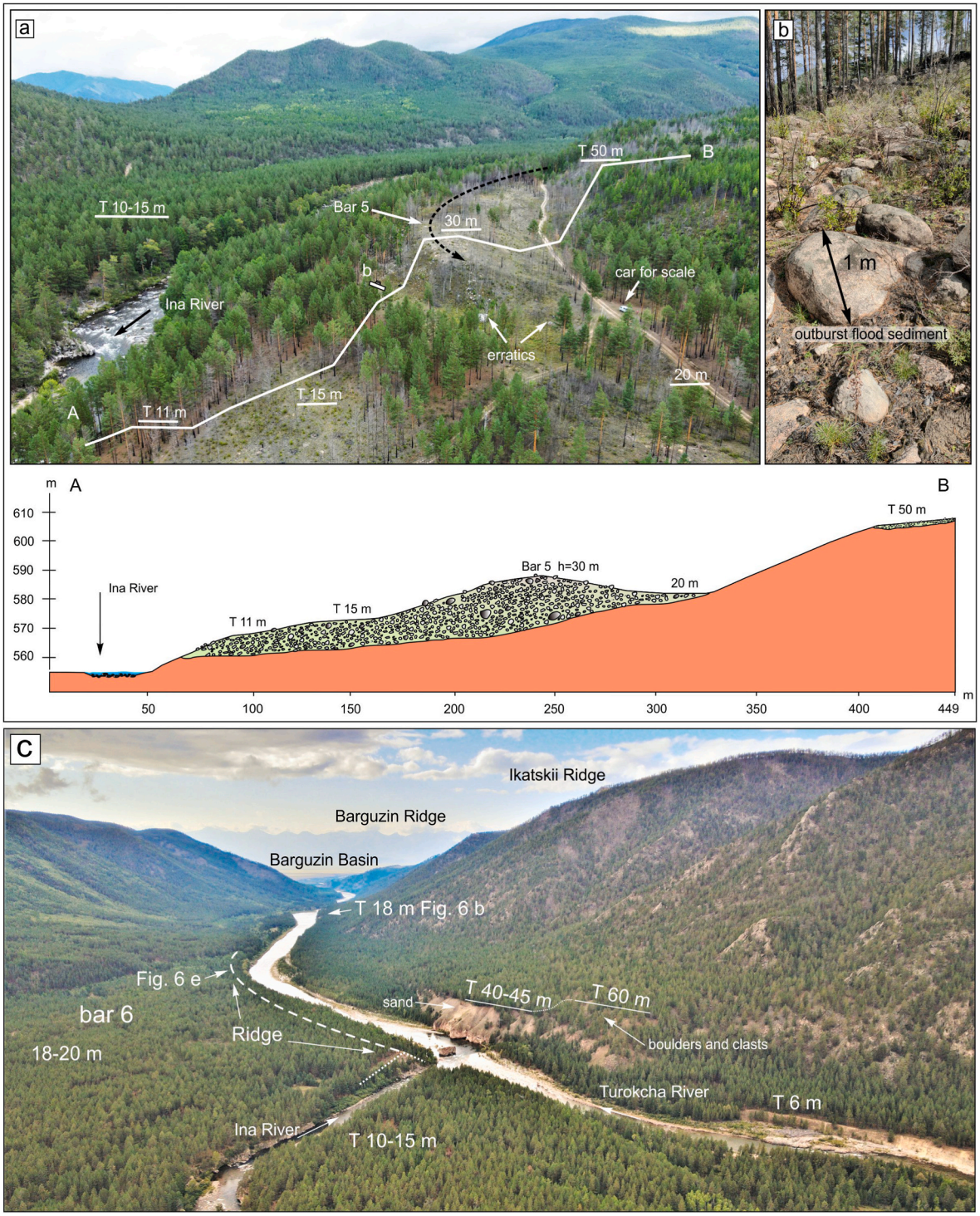

Fig. 3. Location and structure of boulder bar 5 and terraces in the Ina River valley. (a) Terraces of different levels and the structure of boulder bar 5. (b) Boulder bar 5 consists of unsorted coarse clastic sediments capped by sandy - clay sediments. Profile A-B shows the terraces in section. (c) The front of Bar 6, the position of ridge structure and the terraces of different heights.

the Ina and Turokcha river valleys. First, attention was paid to the analysis of the valley slopes for the detection of cirques, rockfalls and landslides. The areas of glacial relief manifestation were also analyzed, including the areas of distribution of terminal moraines. Because one of the hypotheses of IRG formation was the outburst of a dammed lake (Ufimtsev, 1986), special attention was paid to the identification of landforms formed in the area of dynamic impact of the outburst flood. These included terraces, bars, and bedrock islands. It is well established that during an earthquake, especially when it occurs in a mountainous region, slope processes are activated and landslides form over a large area (Adams, 1981, 1981a, 1981b;b; Liu et al., 2019). Therefore, it was important to determine the activity of the faults in our study area. Because strong earthquakes leave significant deformations in the topography, we considered all linear structures that could potentially have been formed by seismogenic movements.

Fieldwork was conducted over several years at key sites. The main

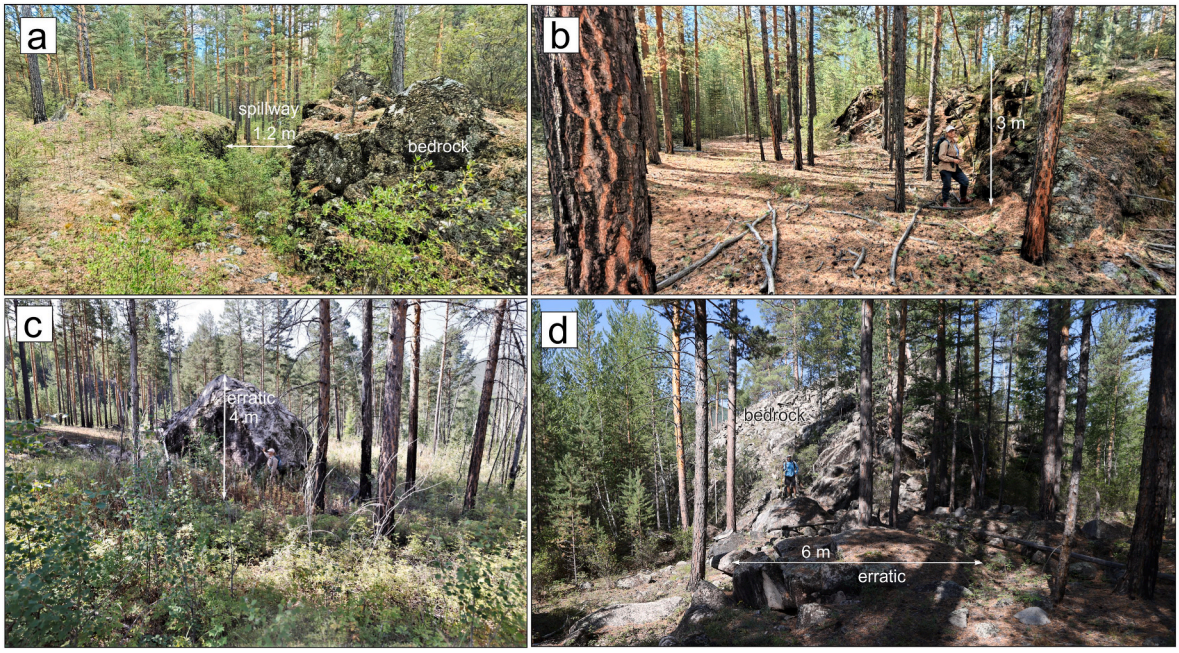

Fig. 4. Topography of Bar 6 (18 m) formed by the Ina outburst flood (spillways, valleys, erratic boulders, and a bedrock island).

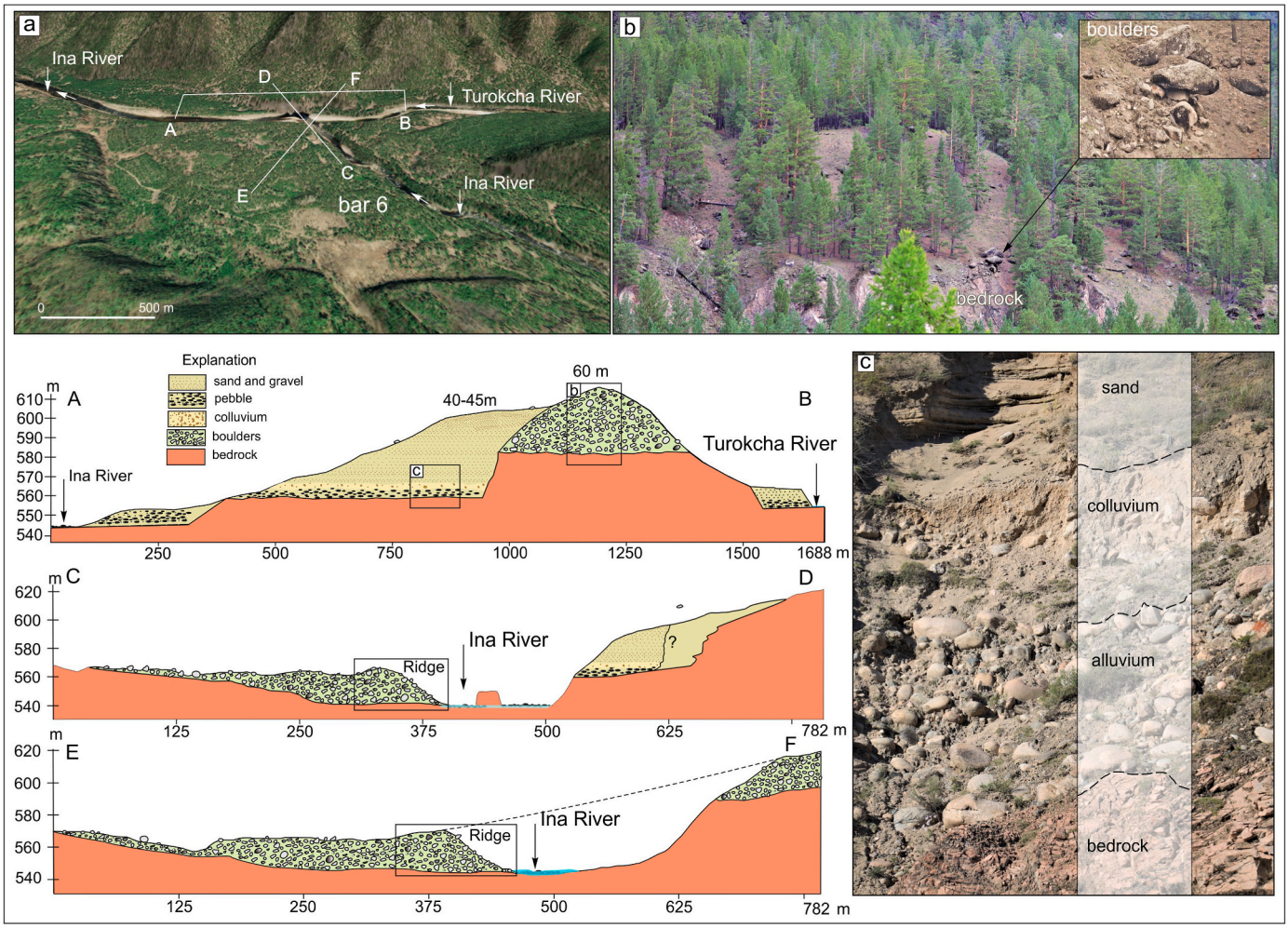

Fig. 5. Bar 6 and deposits of 40-45 m and 60 m on the right bank (a) Location of the profiles. (b) General view and topography of the 60 m terrace. (c) Sediments of the 40-45 m terrace. Profiles A-B, C-D, E-F show sediments of Bar 6 and deposits of 40-45 m and 60 m on the right bank.

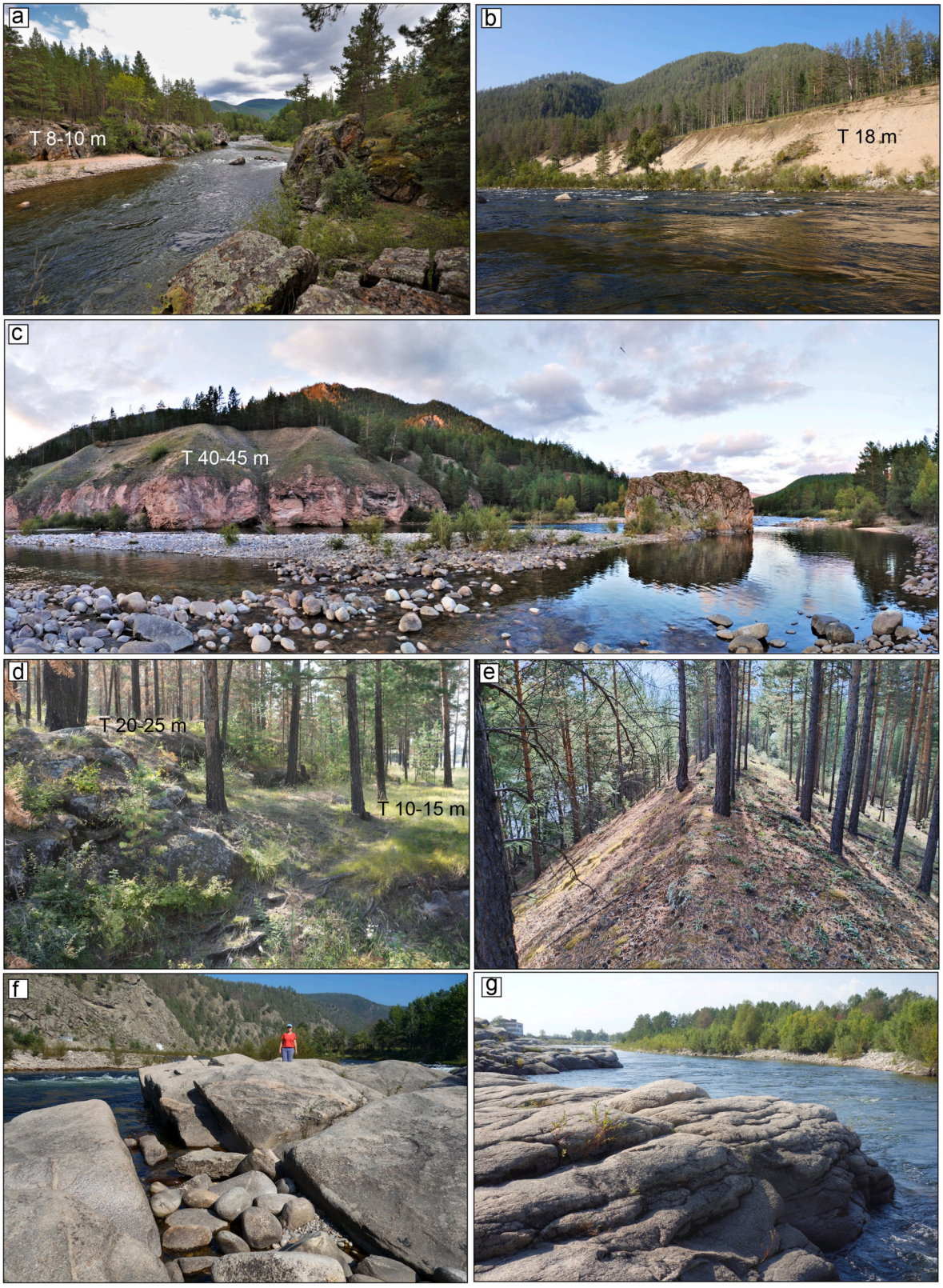

Fig. 6. Landscape formed by the Ina outburst flood. (a) Bedrock terrace formed as a result of changes in the base level during subsidence of the Barguzin Basin. (b) The 18 m terrace composed of sandy sediments. (c) Confluence of the Turokcha and Ina Rivers. A terrace (40-45 m) capped by sandy-silty sediments; note the mid-channel bedrock island. (d) Bedrock terraces at the mouth of the Ina River. (e) Narrow ridge formed by ~ 20 m of erosion, possibly during the falling flood-stages. (f) Fault zone infilled with channel boulders (Ina River). (g) Bedrock terrace (4-5 m) at the mouth of the Ina River.

investigations focused on sections located in the Ina Valley and on the Ikatskii Ridge. A detailed analysis of the parameters and structure of bars, river terraces, and alluvial fans was performed to provide a framework for the evolution of the Ina River valley. During our fieldwork, we examined natural and artificial outcrops of sediments of different origins. Key research points were photographed and documented. Outcrops were cleared for documentation and sampling. The collected samples were processed and analyzed in laboratories for OSL age determination and cosmogenic dating using ^{10}Be and ^{26}Al. By studying satellite imagery and digital elevation model (DEM) data, we created a map (Fig. 2a) that shows the main landforms associated with outburst floods from landslide-dammed lakes in the Ina River valley, from Ina Dam I to the IRG. The map shows boulder bars at heights of 35–40 m, 25–30 m, and 15–20 m, as well as terraces at 4–6 m, 8–10 m, 10–15 m, 15–20 m, 20-25 m and over 50 m. We also identified rockfalls and alluvial fans, as well as seismogenic deformations in the Ukshum fault zone. We identified two areas of landsliding that may be responsible for the formation of dammed lakes: Ina Dam I and Ina Dam II. The heights of the bars and terraces were determined by analyzing cross-sectional profiles. Elevation change boundaries were identified by plotting contour lines at 2-5 m intervals. These contours were then applied to areas of uniform elevation. The reliability of the results is supported by the resolution of the SRTM (30 m), TanDEM-X (12 m), and field observations.

3.1.1. Analysis of the Ina river valley morphology (boulder bars and terraces)

In the Ina River valley, boulder bars begin at Ina Dam I and extend fragmentarily almost to the mouth of the Turokcha River. They have varying shapes (crescent and strip) and sizes. Bar heights range from 35-40 m, 25-30 m, and 15-20 m (Fig. 2a,b,c,d). Bars 35-40 m high are located on the left and right banks of the Ina River near the landslide. Bar 1 originally reached 650 m in length. It was subsequently divided into two fragments by a left tributary. Its maximum width is 100 m. Bar 2 is situated 1 km downstream from the landslide on the right convex bank. It is 1.2 km long and 240 m wide (Fig. 2b). Bars 25-30 m high are located 6, 7.5, and 14 km from the landslide on the left and right banks of the Ina River. Bar 3 is up to 1 km long and 450 m wide. Its surface contains clusters of boulders 1-3, 7-8, and, in one case, 10 m in diameter (Fig. 2c). At its junction with the valley slope, the bar is buried by alluvial fan deposits. Bar 4 is located 7.5 km from the landslide on the right bank and is the largest of the bars (Fig. 2d). It is 2 km long and 460 m wide. Linear scatterings of boulders up to 7-8 m in size are located on the bar's surface, and their orientation is consistent with the valley axis. Bar 5 is located on the left bank, 14 km from the landslide (Figs. 2a and 3a,b,c). It is 500 m long, 150 m wide, and rises to a height of 30 m high on the Ina River side. The bar is not completely adjacent to the slope and is separated from it by a blind valley (Fig. 3a), the bottom of which is 20-22 m above river level. The bar is composed of boulders and coarse gravel (Fig. 3b). The bar's surface is overlain by fine-grained sediments (coarse sand, gravel), resembling saprolite (a weathered granitic crust). Bar 6, 15-20 m high, is located 14.5 km from the landslide. Its length is 1.5 km, and its maximum width is 950 m (Figs. 2 a, 3c). The coarse sediments are 8–10 m thick and overlie bedrock with an uneven contact. The bar surface is characterized by irregularities in the form of paleovalleys and the presence of rare boulders (Fig. 4 a,b, c). An unusual structure for this level is a small mound of bedrock (Fig. 4 d), located in the central part of the bar, measuring 60 × 20 m and 8 m high, with clusters of rounded boulders along the periphery. It should be noted that the height of the bedrock consistently increases from the riverbed to the slope and in some cases appears on the surface of the terrace. This indicates uneven erosional incision both into the surface of the bedrock and subsequently into the sediment cover of bar 6. The frontal part of bar 6 contains an unusually shaped accumulative structure (Ridge Structure) with a maximum relative height of 20 m (Fig. 5). It is a linearly elongated hill with asymmetrical slopes. The ridge consists of poorly sorted pebbles, boulders, and blocks (Fig. 5, profiles CD and EF) and is underlain by a bedrock basement. The hill's height gradually decreases to 7 m downstream, where it forms an extended, pointed ridge (Fig. 6 e). The unusual shape of this part of Bar 6 may be related to linear erosion during the final stage of the Ina outburst flood or to subsequent paleovalley formation.

Opposite the Ridge structure, on the right bank of the Ina River (the confluence of the Ina and Turokcha Rivers), there are fragments of terraces (?) (Fig. 5, profile AB) with edge heights of 40-45 m and 60 m (53.705685°N, 110.334052°E). At the base of the 40-45 m terrace, there is a 7-8 m high bedrock basement overlain by boulder-pebble deposits. Up the section, they are overlain by colluvial deposits and then by coarse-grained horizontally stratified sand (Fig. 5c); the section is capped by subaerial deposits. The 40-45 m deposits of the terrace are adjacent to 60 m high large-boulder deposits, which also overlie bedrock (20 m high). A 4-km-long, 20-25-m-high basement terrace is located before the mouth of the Ina River (Fig. 6 d). Rare boulders and bedrock remnants are found on the surface. A characteristic feature of this area is the presence of transverse faults (striking 280°) that have undergone intense erosion and represent cavities filled with boulders (Fig. 6 f). Faults of this direction are common along a boundary several kilometers wide between the Barguzin Basin and the Ikatskii Ridge (Ufimtsev et al., 2004). A 15-20 m high terrace (53.717522°N, 110.292959°E) is located before the Ina Dam II area (Figs. 3 and 6b). It is composed of horizontally stratified coarse-grained sand and gravel with rare pebbles and boulders (Fig. 6b). The central part of the terrace has been eroded by a lateral tributary. The surface of the terrace in the middle part was covered by deposits of the alluvial fan as a result of which the terrace height (in the axial part of the fan) increased to 24 m. The length of the terrace is 1.5 km, the width is 30-50 m. A 15-m terrace with coordinates (53.687680 N, 110.343594 E) has a similar structure. A 2 m high section was cleared in a roadside cutting. Here, horizontally stratified sands with rare pebbles are also exposed. Two terrace levels, 8–10 m and 4–6 m in height, are sparsely distributed and represent the lower erosional level (Fig. 6a–g).

In summary, 6 bars and a series of terraces with varying parameters were discovered in the Ina River valley, partially overlain by alluvial fans but generally well preserved since their formation. The width of the bars increases with valley widening, while their height decreases with increasing distance from the landslide dam collapse. The presence of other depositional levels along the bar distribution indicates significant subsequent incision into the bar deposits and the formation of terraces. Study of natural outcrops revealed two types of deposits. In the first case, these are poorly sorted packages of boulders and coarse gravel that make up the bars. The second type comprises sand–gravel deposits with weak parallel stratification and inclusions of isolated boulders, mainly forming 10-15 m and 15-20 m terraces or lying as a thin cover on the surface of a 20 m terrace.

3.1.2. Landslide dams and landslide-dammed paleolakes

At a point 24 km upstream from the mouth of the Ina River (53.578476°N, 110.348938°E), a large cirque (900 × 450 m, h = 300 m) was discovered on the right bank, which formed as a result of the destruction of a portion of the valley slope (Fig. 2 a; 7 a, b). Below the detachment scarp, on both the right and left banks are landslide fragments of approximately the same height of 180-190 m (930-935 m a.s.l.). The right-bank landslide fragment is 550 m wide and 500 m long and rests compactly at the base of the detachment wall. The left-bank landslide lies on a slope and has a crescent shape. At the base it has a length of 1200 m, in the upper part 400 m. The combination of these features, such as the location in space, the absence of a detachment scarp on the left bank and, conversely, its presence on the right bank, the same height of the upper part of the landslides, as well as the nature of the distribution of the rock mass on the left bank suggests the existence of a single landslide body with a length of 1200 m. Such examples are widely documented in the global landslide literature, where slope failures,

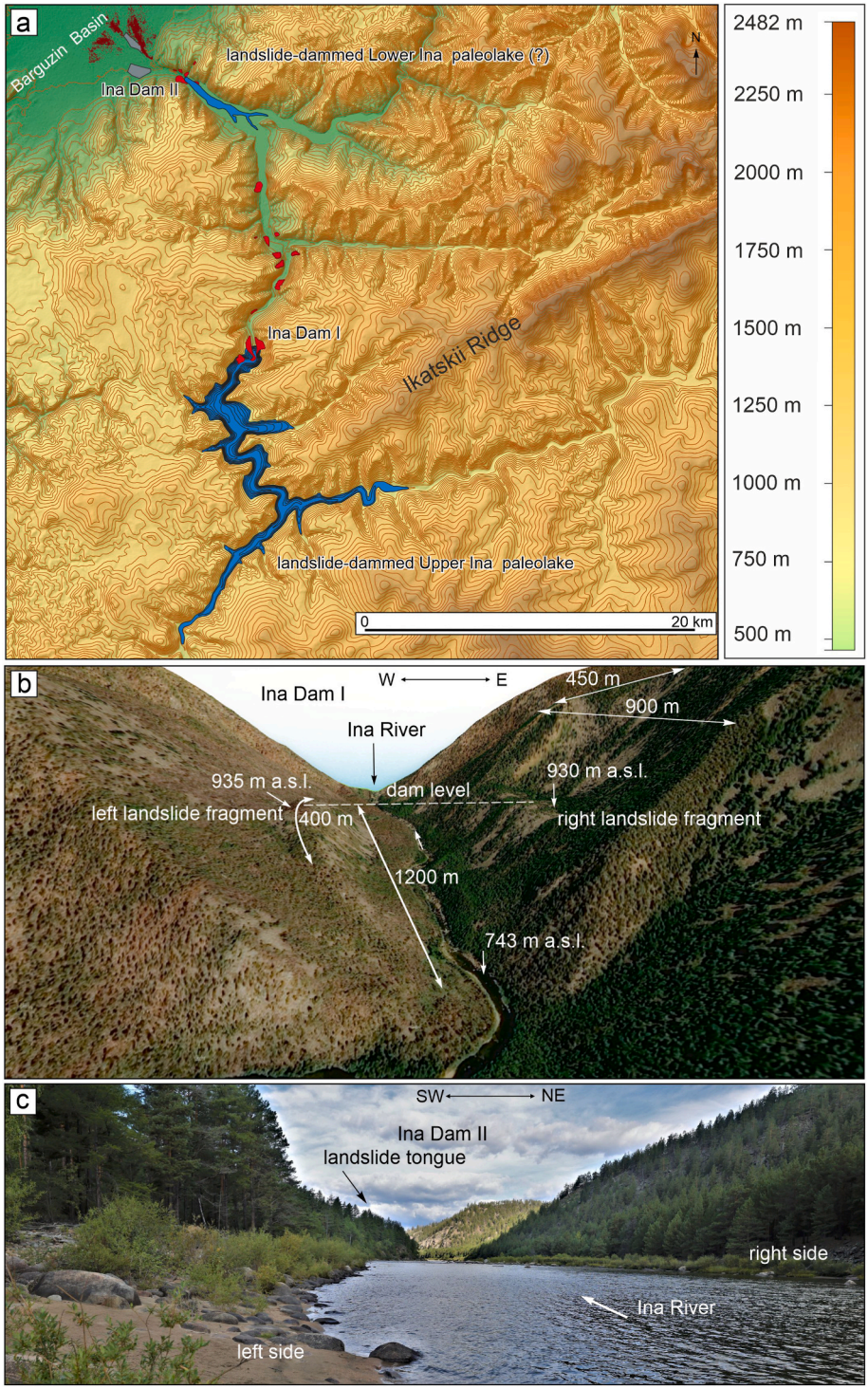

Fig. 7. (a) Map showing the inundated (blue) area of the Ina River valley. Landslides are shown in red. (b) Satellite image (Google Earth) showing details of Ina Dam I. (c) Ina Dam II (see Fig. 2 for location).

formed during strong earthquake, can completely block the valley (Adams, 1981; Costa and Schuster, 1987; Evans et al., 2011, 2011a, 2011b; Strom and Abdrakhmatov, 2018; Liu et al., 2019). We observed a similar landslide scenario within the dynamic influence zone of the Ottugtaygino-Azas Fault (M = 7.5), located in the Sayan-Tuva Highlands (Arzhannikov, 2000). There, in the epicentral zone of a paleo-earthquake, a series of landslides is observed, one of which completely blocks the valley and forms a landslide-dammed lake with similar parameters (Fig. 8). This illustrative example supports and expands our understanding of the mechanisms involved in the formation of landslide-dammed lakes.

The predominant bedrock in this area is Proterozoic granite. Satellite imagery reveals that the landslide dam composed of large fragments with visible diameters reaching 3, 5, 7, and more rarely 10 m. Based on the parameters of the preserved landslide fragments, the dam's volume could have reached 100 Mm^3. If our reconstruction of the collapse is correct, the resulting dam could have impounded a lake 26 km long, with an area of 31 km^2 and a volume of 2.17 km^3 (Fig. 7a).

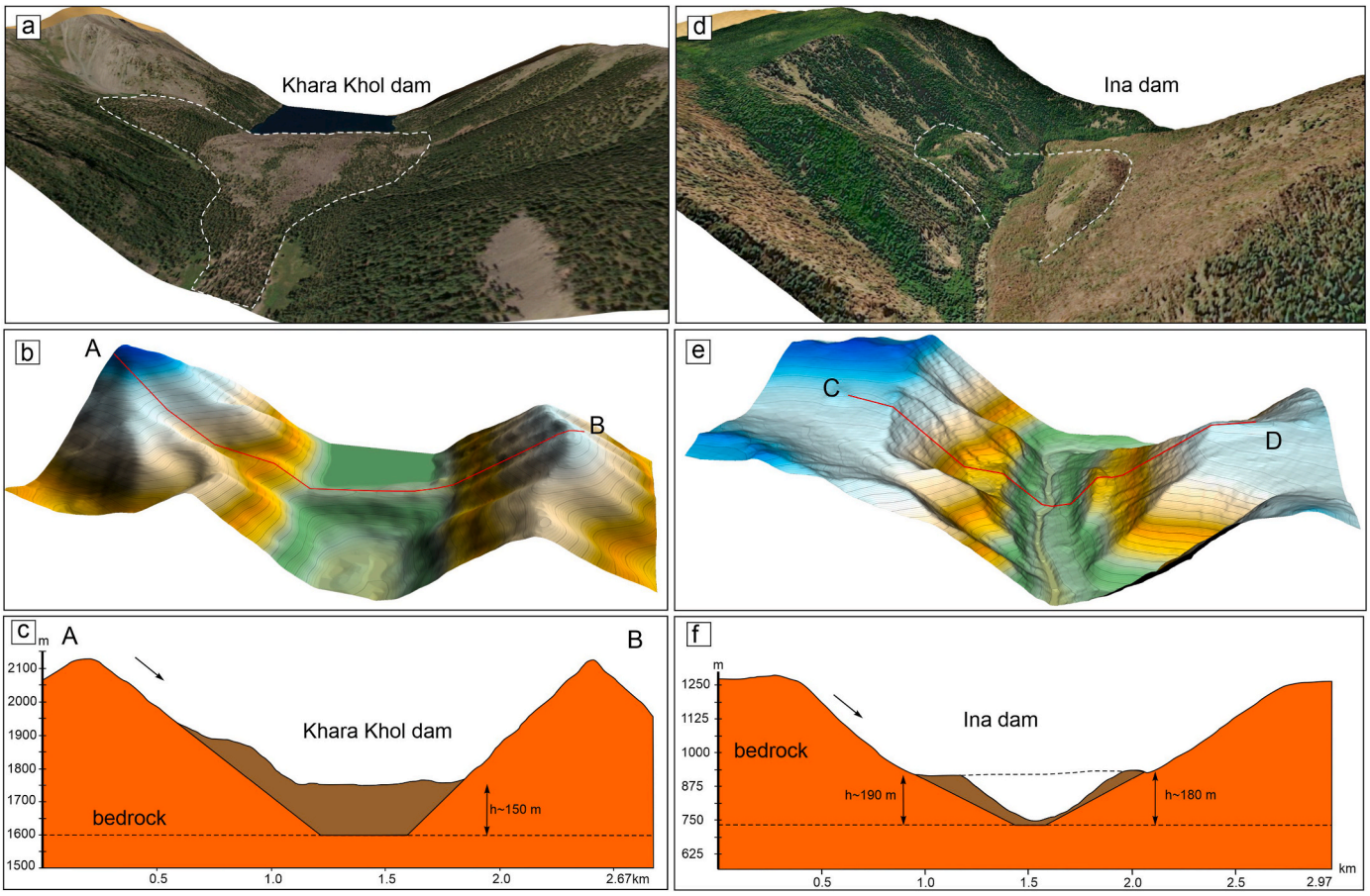

Fig. 8. Comparative geometries of the Khara Khol Dam (Arzhannikov, 2000) (Academica Obrucheva Ridge, Sayan-Tuva Upland) and the Ina Dam I.

An observation point (53.722164°N, 110.273269°E), located 1.5 km upstream from the Ina River mouth, marks the position of two large landslide fragments separated by the modern river channel (Fig. 2a and 7a, c). The left-bank fragment is 900 m long and up to 450 m wide. Reconstruction of its original boundaries based on an analysis of the slope morphology and the boundaries of the debris flow distribution suggests that its original width prior to erosion may have reached 950 m. The right-bank fragment measures 400 × 200 m. Both masses are composed of chaotically distributed large boulders (up to 3–5 m in diameter) of the granitic bedrock that forms the valley sides. These boulders form a distinctive topography with steep frontal slopes and are clearly visible both in riverbank outcrops and on the surface. The main argument for interpreting them as a single landslide body is their symmetrical distribution on both sides of the valley narrows and their identical lithology. Further indirect evidence supporting the hypothesis of a major landslide in this part of the Ina River valley is the patchy distribution of large boulders, which are separated by sections with minimal boulder abundance. For example, between Bar 6 and the IRG, there is a reach where large boulder clusters are absent in the river valley, yet they are abundantly widespread on the alluvial fan of the IRG. This suggests the existence of a large landslide near the river mouth, which served as the source for the boulders in the IRG. Moreover, the IRG alluvial fan exhibits an increase in both the concentration and size of granitic boulders that are lithologically similar to the landslide clasts. This discontinuous, focal distribution is inconsistent with gradual fluvial transport and instead points to a single, massive influx of debris from a point source, logically interpreted as a large landslide. The thickness and areal extent of the boulder clusters within the IRG fan indicate an initial landslide or rock avalanche volume sufficient to have completely blocked the valley in the study area.

The formation of such a large landslide dam could have led to the impoundment of a paleolake. An indirect indicator of this process is the sand and gravel deposits forming an 18 m high terrace located 500 m upstream of the landslide. However, the origin of these deposits allows for two main interpretations: they could have formed either in a lake that was dammed upstream of the landslide (e.g., as deltaic deposits) or during an outburst flood of the Ina River (e.g., as slackwater deposits on a 15-m terrace upstream of Bar 5). Thus, the genesis of the terrace deposits is ambiguous. The presence of identical granitic bedrock in the landslide fragments on opposite banks of the Ina River, as well as similar boulders within the IRG, strongly suggests a temporary damming of the Ina River valley and the possible formation of a paleolake. However, its estimated size and configuration, reconstructed using a digital elevation model, remain hypothetical and require further verification through detailed lithological analysis and geochronological dating of the deposits (Fig. 7a).

3.1.3. *Ina Rock Garden*

The study area is located on the boundary between the Barguzin Basin and the Ikatskii Ridge within the Ina River valley (Fig. 10). At the river's exit from the ridge lies one of the largest alluvial fans of the Barguzin Basin (area ~40 km^2), composed of various sediment fractions, including large boulders reaching several meters in diameter. The distribution of these boulders extends from the Ina River valley toward the Barguzin Basin (Fig. 10a). The source of the boulders may have been Ina Dam II and granite outcrops located at the mouth of the Ina River. Several boulder clusters are clearly visible in the satellite imagery. These consist primarily of angular, poorly rounded granite boulders reaching 9-10 m in size. Their spatial distribution indicates a significant energy input during their transport. The boulders and blocks do not form a

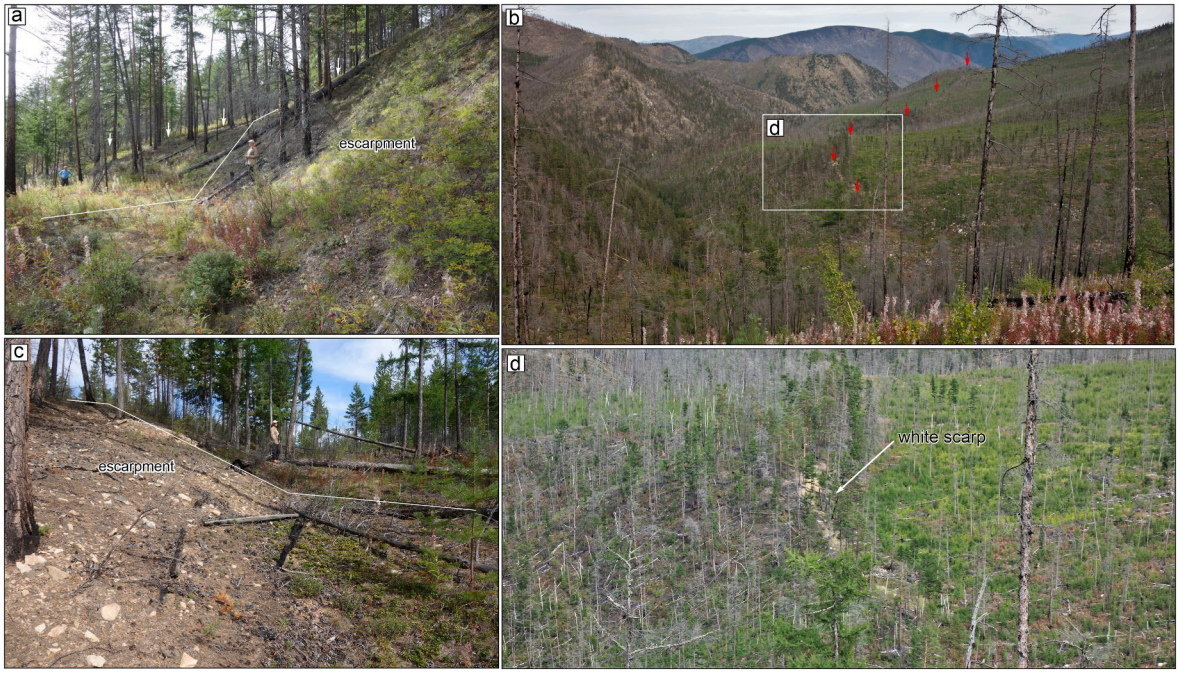

Fig. 9. A seismogenic scarp formed in the epicentral area of a large paleoearthquake in the Ukshum fault zone (a, b, c, d).

continuous cover, but are spaced apart, with the intervening material consisting of sand, gravel, and pebbles. The maximum advance of boulder material into the Barguzin Basin is recorded at a distance of up to 3.7 km on the left bank and 5.9 km on the right bank of the Ina River. Individual boulders are observed at distances of up to 8.5-9 km. Sands, intensively reworked by aeolian processes, are widespread along the periphery of the alluvial fan. Based on the orientation of the linear dunes, the prevailing wind direction is from the southwest to the northeast. Several boulder fields are identified on the left and right banks of the Ina River. Because the left bank is significantly higher than the right bank, the distribution of the boulder fields is uneven. A network of paleochannels, directed north to northeast, covers the entire alluvial fan.

On the right bank of the Ina River, the largest accumulation of boulders extends for over 5 km, with an average width of 3–4 km (Fig. 10 a, b, d). Boulders are scattered across the area. The highest frequency of fragment concentration and accumulation occurs within the first 400 m from the point where the Ina River exits the Ikatskii Ridge. The largest specimens, some of which reach up to 15 m in length are located in this field (Ufimtsev et al., 2004). However, the description by Ufimtsev et al. (2004) contains an inaccuracy: the boulder named "Ship" (53.742620°N, 110.227009E) is actually 32 m long, 12 m wide and 2.5 m high (Fig. 10e). The minimum weight of this granite block is estimated at 1500 tons. It is located nearly 2 km from the river's exit point from the Ikatskii Ridge, in the center of the settlement of Ina Village within a private garden. Literature sources document the transport of boulders of comparable size. For example, combined flooding from the Min River and Songping Valley (July 28, 1992) entered Xiao Lake, triggering an outburst flood and transporting a 600 m^3 boulder 310 m downstream (Wang and Wang, 2005; Chen, 2014; Liu et al., 2019). Further downstream, the distribution frequency decreases, and the space between individual boulders increases. At a distance of 2.5 km from the point where the river exits the mountains, the continuous distribution of debris gives way to isolated clusters. The maximum distance at which isolated bedrock blocks are observed exceeds 9 km. The boulders are primarily composed of granite and exhibit rough, angular edges, indicating a short transport distance. It is possible that the source of the IRG was Ina Dam II, which was eroded and the debris subsequently transported by the flood.

On the left bank, the accumulation of boulders begins approximately 2 km from the point where the Ina River exits from the Ikatskii Ridge (Fig. 10 a, c). Here, the elevation of the right and left banks become similar, and the flow is distributed over a larger area. The distribution of debris on the left bank is characterized as solitary, with the main mass dispersed over an area of about 1 km^2. The diameter of some blocks is 9-10 m. A sharp decrease in boulder distribution toward the Barguzin Basin was probably caused by an existing pingo field oriented transverse to the flow direction. Beyond this zone, isolated boulders are observed at a maximum distance of up to 6 km. According to Ufimtsev (1986), the thickness of flood deposits in the axial part of the alluvial fan 2.5 km from the outlet of the Ina River from the Ikatskii Ridge is 6 m. At a distance of 4 km from the river exit, a 2.5 m thick horizon of flood deposits was exposed in a quarry on the left bank of the Ikatskii Ridge, on the periphery of the alluvial fan. The upper part of the unit consists of pebbles and small angular rock fragments 0.25-0.3 m thick, followed by a horizon of blocks and rounded boulders. The matrix between them consists of unsorted, unrounded sand derived from weathered granite. This layer is 2.2 m thick. Below it lies a paleosol developed over clays (Ufimtsev, 1986).

3.2. *Paleoseismological investigations*

Because landslide formation can be associated with strong earthquake shaking, we applied a paleoseismological method (Solonenko, 1962; McCalpin, 1996) that allows for the identification of source zones of strong paleoearthquakes through satellite imagery and field surveys. This method is based on the detection of paleoseismogenic deformations within fault zones. When tectonic stresses are released during an earthquake, the earth's crust ruptures. Under certain conditions, this rupture is expressed in the topography as linear scarps (ranging from a few kilometers to hundreds of kilometers) and a series of micrograbens. Such deformations are typically obliterated rapidly in large valleys and within alluvial fans. However, they are well preserved on slopes, watersheds, ephemeral stream thalwegs, and terrace surfaces. This method provides information on fault activity, the location of strong earthquake epicenters, the seismic hazard of the area, and the likelihood of coseismic gravitational processes manifesting as rockfalls and landslides. Satellite imagery reveals the presence of seismogenic features within the

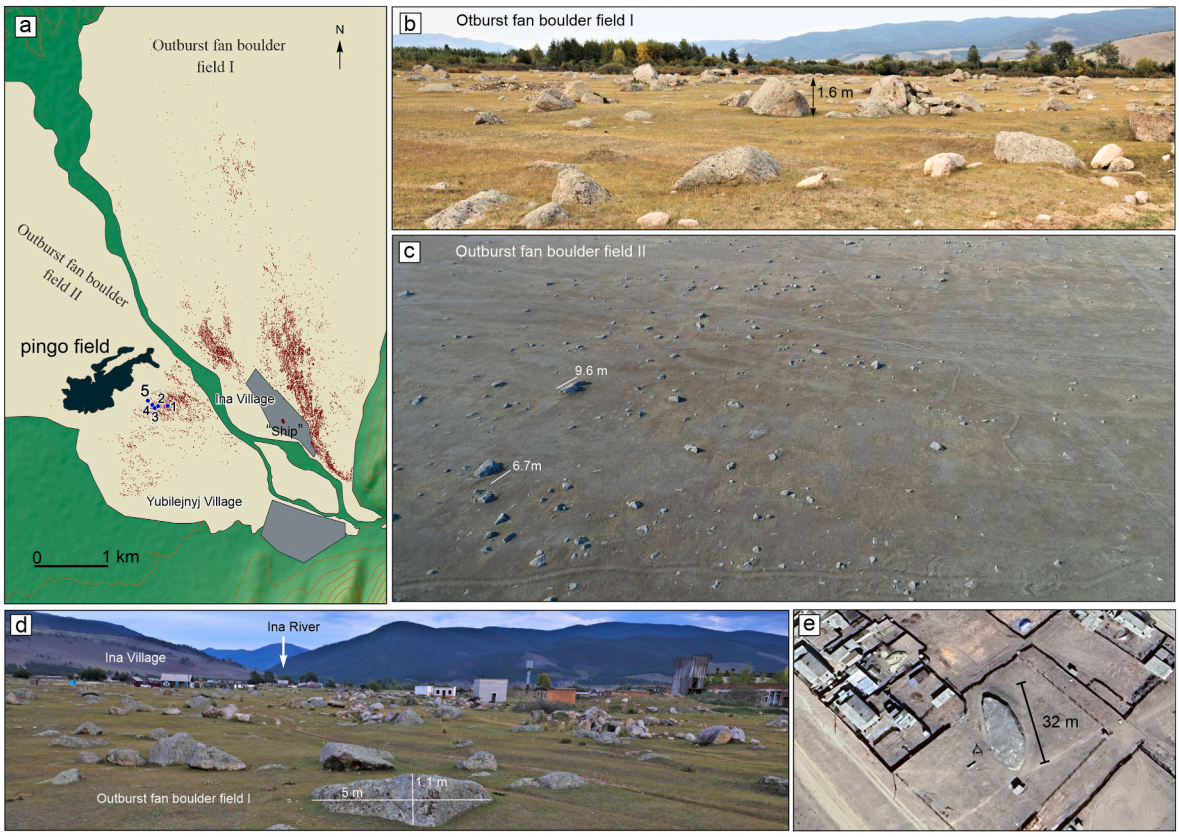

Fig. 10. The Ina Rock Garden. (a) Outburst boulder fields in the Ina River valley. (b, c, d) Field photographs of boulders. (e) Giant boulder ("Ship") in the center of the Ina Village (satellite image, Google Earth).

Ukshum fault zone (Figs. 2 and 9). The activated fault segment appears as scarps located on slopes of various aspects and is interpreted as the epicentral area of the paleoearthquake. It is 8 km long and likely extends into the Akuli River valley, where left-lateral displacement of a series of watershed spurs is recorded, and into the Suvokan River valley, where seismogenic reactivation has also been observed on the slopes.

The Ukshum fault (Fig. 2a) originates on the northwestern slope of the Ikatskii Ridge and can be traced in the Suvokan River valley, in the upper reaches of the Levyi Bodon, Pravyi Bodon, and Karamina rivers, and further east along the Ushman and Akuli river valleys. Its strike is 85°, dip direction 355°, and dip angle 85° (Lunina and Gladkov, 2007). According to geological survey data, the fault length reaches 45 km (Gusev and Shobogorov, 1979). Mylonitized zones, slickensides, and dikes are common within its internal structure. The fault zone width reaches 2 km. Field observations of deformations have shown that the fault displaces young landforms such as ephemeral stream valleys, floodplains, and terraces (Fig. 9a, b, c, d). The fault scarp forms dams across the valley of ephemeral stream channels. The magnitude of the paleoearthquake that caused the surface deformations is typically estimated using empirical relationships derived from the parameters of modern and historical earthquakes (Wells and Coppersmith, 1994). Based on the fault parameters, and assuming the entire length of the fault (45 km) represents the seismogenic rupture, we obtain an estimated moment magnitude of M ~ 7.

3.3. Maximum discharge calculation methods

Studying the various characteristics of outburst floods from landslide-dammed lakes is essential for mitigating the risk of natural disasters. A key parameter of such floods is the peak discharge (Q). Regression analyses by various authors (Costa, 1985; Evans, 1986; Costa and Schuster, 1987; Liu et al., 2019) utilize different parameters: the volume of water released from the lake (V), dam height (H), breach depth (h), the dam factor (H × V), and potential energy (PE). These analyses provide empirical formulas applicable to both contemporary catastrophic events and paleohydrological and sedimentological reconstructions. As presented in Table 4, estimates for the maximum discharge of the Ina outburst flood vary by a factor of several times depending on which empirical relationship (Costa, 1985; Evans, 1986; Costa and Schuster, 1987; Liu et al., 2019) and associated parameters are used, which significantly complicates a reliable assessment.

According to Costa (1985), the most effective independent variable for reconstructing paleoflood peaks resulting from natural dam failures is the dam factor (height multiplied by volume H × V). Applying this relationship to the Upper Ina landslide-dammed paleolake, which had a water volume (V) of 2.17 km^3 and a dam height (H) of 180 m for Ina Dam I, the peak discharge is estimated to be approximately 4.6 × 10^4 m^3/s. Evans (1986) derived an empirical logarithmic relationship between maximum discharge (Q) and outburst flood volume (V) based on data from constructed dam failures. Given that data from landslide dam failures fall within the 95% confidence interval of this relationship, it can also be applied to such events. In this case, the calculated peak discharge is approximately 6.4 × 10^4 m^3/s. To reconstruct maximum discharge in paleohydrological or sedimentological studies, Costa and Schuster (1987) proposed using potential energy (PE, in joules), calculated as PE=HV9800. Using this approach, the peak discharge for the Ina outburst flood is estimated to be approximately 3.9 × 10^4 m^3/s. More recently, Liu et al. (2019), based on an analysis of reliable parameters from 10 historical outburst floods, proposed an empirical relationship between Q and the breach depth, the volume of discharged water, and their product. Applying their relationships to the parameters of the Ina event yields Q values ranging from 8.4 × 10^4 m^3/s to 19.8 × 10^4 m^3/s. Liu et al. (2019) emphasize that the product of volume and breach depth (V×h) is the most reliable parameter for determining Q, which in this

Table 1
Location and boulder geometry of the Ina samples.

Sample	Latitude	Longitude	Altitude (m a.s.l)	Boulder size (l x w x h) (m)	Kind of rock
Ina - 18 - 1	53.742650	110.208450	505	6.0 x 4.6 x 2.2	granite
Ina - 18 - 2	53.742567	110.206417	507	4.2 x 4.6 x 1.6	granite
Ina - 18 - 4	53.742867	110.205383	509	9.0 x 6.7 x 1.6	granite
Ina - 18 - 5	53.743217	110.204667	508	3.8 x 3.0 x 1.0	granite

case gives an estimated maximum discharge of 13.2 × 10^4 m^3/s. Based on the range of estimates from these various empirical relationships (Costa, 1985; Evans, 1986; Costa and Schuster, 1987; Liu et al., 2019) and their closest alignment with parameters from historical events, it can be inferred that the maximum discharge of the Ina outburst flood likely ranges between 3.9 × 10^4 m^3/s and 13.2 × 10^4 m^3/s.

3.4. Sample collection and dating

3.4.1. ^{10}Be, ^{26}Al dating

We applied cosmogenic nuclide dating (^{10}Be, ^{26}Al) (Stone, 2000; Gosse and Phillips, 2001; Merchel and Bremser, 2004) to determine the age of exposed boulders within the outburst fan and to reconstruct the exposure history of each sample. One of the main prerequisites for obtaining reliable data in cosmogenic dating is the stability of the dated boulder since the time of its exposure. The stabilization time of the boulder should coincide with the moment of its final emplacement within the zone of dynamic influence of the outburst flow, and its position (spatial orientation) should remain undisturbed until sampling. Several factors were considered when selecting sampling sites: the absence of forest cover (snow cover depth increases significantly in forested areas), the presence of a flat stable surface on which the boulder rests, and the size of the boulder (Table 1). On the left bank of the Ina River, within the outburst fan boulder field II, we selected four weakly abraded boulders from which samples were collected (see Table 2 for sample details). Samples were collected from the upper surface of the boulders using a hammer and chisel (Fig. 11). Sample thickness was typically 2-3 cm. Coordinates were recorded using a handheld GPS receiver with an accuracy of ±3 m. The topographic shielding of the sampling site with respect to the cardinal directions was also recorded.

3.4.1.1. Samples preparation and measurements; exposure ages calculation. ^{10}Be and ^{26}Al samples preparation followed the classical preparation steps as described in (Brown et al., 1991) for ^{10}Be in quartz. For all samples for ^{10}Be measurements an in house prepared beryllium phenakite carrier (Merchel et al., 2008) was used (~0.10 g with a [^{9}Be] of (3025 ± 9) ppm). For ^{26}Al samples, as the native ^{27}Al concentrations (measured by a Thermo ICAP 6500 ICP-OES) were sufficient, no spike was added.

After being oxidized for 1 h at 700°, BeO and $Al2O_3$powders were mixed with niobium powder and silver respectively and packed in copper cathodes prior to AMS measurements. Measurements were performed at the French Accelerator Mass Spectrometry (AMS) National Facility "ASTER" located at CEREGE in Aix-en-Provence, France (Arnold et al., 2010).^{10}Be data were calibrated from an ASTER in-house preparation "STD11", with a^{10}Be/^{9}Be ratio of (1.191 ± 0.013) x 10^{-11} (Braucher et al., 2015) using a^{10}Be half-life of (1.387 ± 0.0012)x10^6 years (Chmeleff et al., 2010; Korschinek et al., 2010). Aluminum

Table 2
Summary of cosmogenic nuclide data.

Samples	Depth (cm)	10Be (at/g)	Age (ka)	26Al (at/g)	Age (ka)
Ina-18-1	0	62,354 ± 6280	9.96 ± 1	407,528 ± 20,688	9.12 ± 0.46
Ina-18-2	0	66,210 ± 9895	10.54 ± 1.58	509,130 ± 50,446	11.4 ± 1.13
Ina-18-4	0	325,092 ± 102,673	49.76 ± 15.72	1,955,176 ± 70,775	44.43 ± 1.61
Ina-18-5	0	34,691 ± 8587	5.78 ± 1.43	203,405 ± 10,886	4.53 ± 0.24

Fig. 11. Large granite boulders from which samples were collected for cosmogenic (^{10}Be and ^{26}Al) dating (Barguzin Basin, Outburst fan boulder field II).

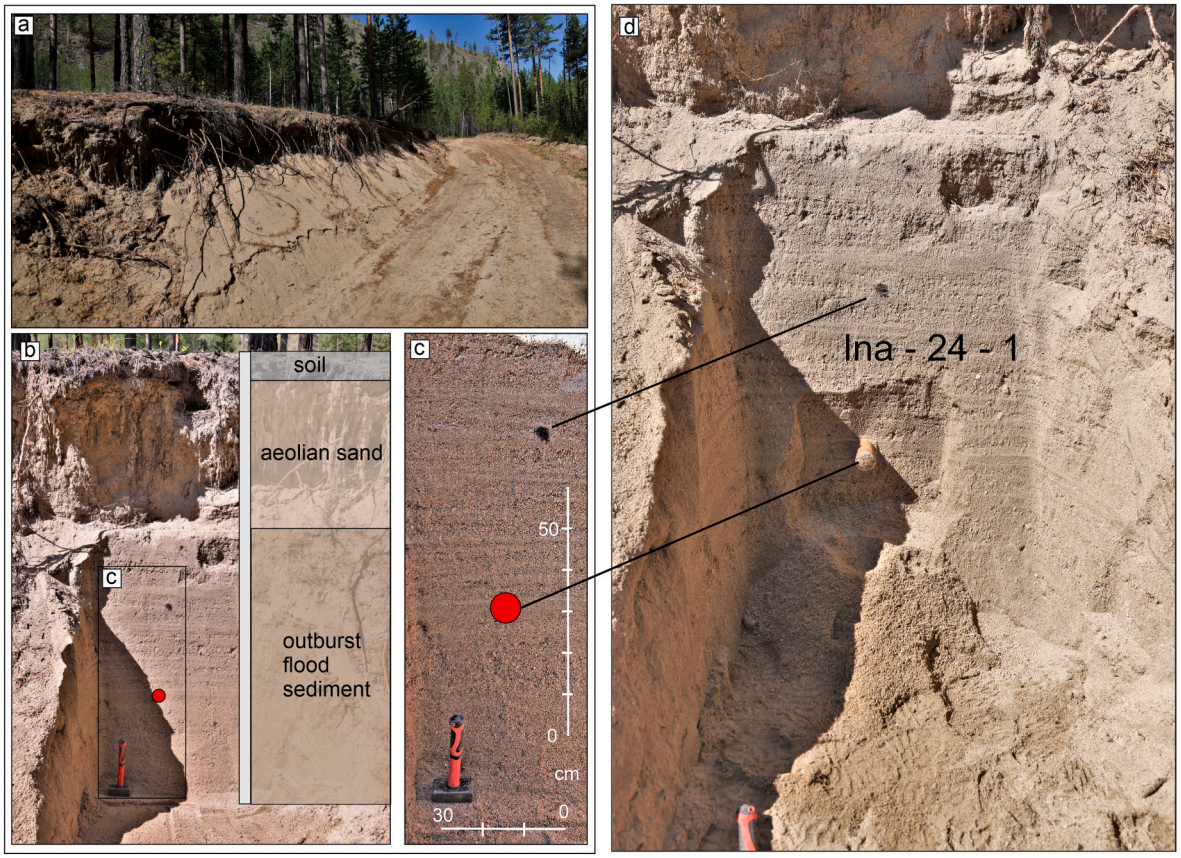

Fig. 12. Channel margin (a) and flood sediments of the 15 m terrace upstream of Bar 5. (b, c) Sand and gravel deposited by the Ina outburst flood. (d) Sample collected for OSL dating (see Fig. 3 for location).

measurements were performed against an in-house standard called SM-Al-11.with $^{26}Al/^{27}Al = (7.401 \pm 0.064) \times 10^{-12}$ which has been cross-calibrated against the primary standards certified by a round-robin exercise (Merchel and Bremser, 2004). Analytical uncertainties (reported as 1σ) include uncertainties associated with AMS counting statistics, AMS external error (0.5% for ^{10}Be), chemical blank measurement, and, regarding ^{26}Al, ^{27}Al measurements.

The general equation used to model ^{10}Be or ^{26}Al concentrations considering the three types of particles involved is given by eq. (1):

$$N(x,\varepsilon,t) = \frac{P_n.e^{-\frac{\rho x}{\Lambda_n}}.\left(1\text{-}e^{\left(-t\left(\frac{\rho\varepsilon}{\Lambda_n}+\lambda\right)\right)}\right)}{\frac{\rho\varepsilon}{\Lambda_n}+\lambda} + \frac{P_{slow}.e^{-\frac{\rho x}{\Lambda_{slow}}}.\left(1\text{-}e^{-t\left(\frac{\rho\varepsilon}{\Lambda_{slow}}+\lambda\right)}\right)}{\frac{\rho\varepsilon}{\Lambda_{slow}}+\lambda} + \frac{P_{fast}.e^{-\frac{\rho x}{\Lambda_{fast}}}.\left(1\text{-}e^{-t\left(\frac{\rho\varepsilon}{\Lambda_{fast}}+\lambda\right)}\right)}{\frac{\rho\varepsilon}{\Lambda_{fast}}+\lambda} + N(0,\varepsilon_2,\infty).e^{-\lambda t} \quad \text{(eq.1)}$$

where $P_{n.}$, $P_{stop.}$ and P_{fast} are the production of neutrons, stopping and fast muons respectively, ρ is the material density, ε is the denudation rate, t is time, Λ_{neut}, $\Lambda_{stop.}$ and Λ_{fast} are the attenuation lengths of neutrons (150 g/cm^2) and stopping (1500 g/cm^2) and fast muons (4320 g/cm^2), respectively. The term $N(0,\varepsilon_2,\infty)$ is a potential inheritance coming from a previous exposure at steady state (T = infinite) and with a denudation ε_2. λ is the radioactive decay constant (λ = ln2/half-life). Muon contribution scheme follows (Braucher et al., 2011). A sea level high latitude spallation production rate of 4.02 ± 0.32 at. g^{-1} a^{-1} (Borchers et al., 2016) was used and scaled using (Stone, 2000). The spallation production ratio $^{26}Al/^{10}Be$ used at ASTER is 6.61 ± 0.50.

The exposure ages obtained from the samples revealed a wide range, from ~5.8 ka to ~50 ka. The locations and dimensions (Table 1) of the dated boulders rule out post-depositional rotation or spatial displacement, suggesting that other factors likely account for the observed age discrepancy. Our analytical approach enables age estimation using two independent nuclides (^{10}Be, ^{26}Al), whose production rates differ by a factor of 6.61 ± 0.50. A significant disagreement between ^{26}Al ages and ^{10}Be ages would indicate a complex exposure history for the boulder in question. Samples Ina-18-1, 2, and 5 yielded similar ^{10}Be and ^{26}Al ages (Table 2), suggesting a simple exposure history. In contrast, sample Ina-18-4 exhibits a significant discrepancy between its ^{10}Be and ^{26}Al ages (Table 2). This discordance points to possible multiple episodes of exposure and burial. Consequently, we exclude sample Ina-18-4 from consideration in determining the age of the Ina outburst flood. Among the remaining samples, Ina-18-1 and Ina-18-2 yield the most concordant ages. Sample Ina-18-5 yielded the lowest exposure age within this group (approximately half that of Ina-18-1 and Ina-18-2). This younger age may be attributable to shielding or high denudation rates.

Table 3
Optically stimulated luminescence (OSL) summary for quartz and Feldspar (Fs) extracts.

N°	Lab. no.	Field no.	Mineral	Depth (m)	w.c. (%)	Sand size fraction (μm)	n	Specific activity (Bq kg^{-1})				Dose rate (Gy ka^{-1})	Protocol	Equivalent dose (Gy)	OD %	Age (ka)
								^{238}U	^{226}Ra	^{232}Th	^{40}K					
1	RGI-1362	INA-24-1	Q	1.5	31	180-250	14/10	19 ± 3	20.9 ± 0.4	29.6 ± 0.5	851 ± 46	2.83 ± 0.12	pIR OSL	26.0 ± 5.7	66	**8.7 ± 2.0**
			Fs			180-250	85/0/100					3.70 ± 0.21	IR_{50}	74 ± 10	59	
							37/48/100						$pIR_{50}IR_{290}$	45 ± 13	103	**12 ± 4**

Depth is the current burial depth, w.c. is the saturated water content and n is number of aliquots included in the dose estimation. The equivalent doses are estimated using the arithmetic mean. The values of specific activities of radionuclides, equivalent dose, dose rate and age are given with a standard measurement error (1σ). Equivalent dose for feldspars was determined based on single grains.
Due to large overdispersion (OD) values, the Minimum Dose Model (MNDM) or Minimum age model (MAM)(Galbraith et al., 1999) was chosen for age calculation. Overdispersion most often indicates uneven zeroing of sample grains.

Table 4
Methods for calculating the maximum discharge from data (Costa, 1985; Evans, 1986; Costa and Schuster, 1987; Liu et al., 2019).

H	V	HV	PE	Reference
-	-	Q = 181 $(HV^*)^{0.43}$ (45,932 m^3/s)	-	Costa (1985)
-	Q = 0,72$V^{0,53}$ (64,000 m^3/s)	-	-	Evans (1986)
-	-	-	Q = 0.0158 $(PE)^{0.41}$ (38,696 m^3/s)	Costa and Schuster (1987)
Q = 33.951 $h^{1.670}$ (198,205 m^3/s)	Q = 0.024 $V^{0.701}$ (84,153 m^3/s)	Q = 0.083 $(Vh)^{0.535}$ (131,916 m^3/s)	-	Liu et al. (2019)

Q = maximum peak flood discharge (m^3/s); V = volume of water released from the lake (m^3) (Liu et al., 2019); V* = volume of water released from the lake (m^3x10^6) (Costa, 1985); H = height of the dam (m); h = breach depth (m); HV = dam factor; PE = potential energy, in joules (PE=HV9800).

3.5. OSL dating

The distribution of sand and gravel deposits downstream of the landslide in the Ina River valley is quite extensive. One promising sampling location is an 18-20 m high terrace situated below the confluence of the Ina and Turokcha Rivers. However, this terrace lies within the area proposed for the lower lake, which could potentially bias the age estimate for the Ina outburst flood. Therefore, we collected sample Ina-24-1 from a 15 m high terrace (Figs. 2a and 12). A roadside outcrop on the slope of this terrace exposed horizontally layered yellow-grey sand and gravel. The sample was collected from the upper part of the terrace at a depth of 1.5 m, at coordinates 53.686183° N, 110.343983° E (Fig. 12c and d). For luminescence dating, the sample was collected by hammering a steel tube (approximately 5 × 30 cm) into a freshly cleaned vertical section. The tube ends were immediately sealed airtight with plastic tape to preserve in situ moisture content. Sample preparation and OSL dating were conducted at the OSL Laboratory of the A.P. Karpinsky All-Russian Geological Research Institute, St. Petersburg. Sample preparation was carried out under subdued red-light conditions following standard protocols (Murray et al., 2021). OSL dating of sample Ina-24-1 (Table 3), taken from a 15 m high terrace, yielded ages 8.7 ± 2.0 ka for quartz and 12 ± 4 ka for feldspar. Within error, these ages are considered reliable and can be used for the reconstruction of the Ina outburst flood.

4. Discussion

4.1. The cause of the formation and collapse of Ina Dam I and the formation of the Ina outburst flood

The primary triggers of landslide formation are precipitation and earthquakes (Adams, 1981; Costa and Schuster, 1987; Evans et al., 2011; Fan et al., 2012a, 2012b; Liu et al., 2019). As the study area is composed mainly of granite and ancient crystalline schists, precipitation is an unlikely cause of the large landslides observed. However, the region is characterized by high seismic potential, which, combined with high, steep slopes, creates favorable conditions for their formation. Based on our research, we associate the formation of dammed lakes in the Ina River valley with large landslides, which are widespread here over a distance of 24 km. We propose that the destruction of the valley slopes occurred as a result of fault reactivation and strong paleoearthquakes (Chipizubov et al., 2007). The sources of strong paleoearthquakes could have been the Barguzin fault (L = 200 km, M = 7.5-8) (Chipizubov et al.,

2007) and the Ukshum fault (L = 40 km, M = 7). Given these magnitudes and typical focal depths of 15-20 km for the earthquakes, the macroseismic equation for the Baikal region (Shebalin, 1968) yields a predicted shaking intensity in the Ina Dam I area of I = 8.7 for an M = 7.5 event and I > 9 for an M = 8 event originated from the Barguzin fault. For the Ukshum fault, an M = 7 event could also produce a shaking intensity of I > 9.

Two possible causes of dam failure are typically considered: erosion from overtopping (Costa and Schuster, 1987) or earthquake-induced failure (Liu et al., 2019). Dam failure due to erosion occurs when the dam is composed of densely packed, low permeability rock debris, which prevents significant water filtration. As the impounded lake fills, the water eventually overtops the dam crest, leading to erosion and eventual collapse. In the case of Ina Dam I, the dam debris consists of large granite boulders, which would have facilitated water seepage through the dam body. This permeability would likely have prevented the paleolake from overtopping and thus averted dam failure due to erosion. Therefore, the more likely cause of failure for Ina Dam I is the repeated impact of strong paleoearthquakes.

4.2. Outburst flood sediment formation in the Ina river valley

The formation of boulder bars and terraces (Fig. 2) during the Ina outburst flood was a complex geomorphological process. Initially, powerful turbulent flows capable of detaching and transporting large boulders emerged during the flood (Liu et al., 2019; Turzewski et al., 2019; Wu et al., 2020). The lower part of the flow was dominated by coarse sediments (blocks, boulders, and coarse gravel), whereas the middle and upper parts were rich in sand and fine gravel. As the flow velocity decreased, the particles settled, forming deposits of varying sizes and compositions. Because the width and geometry of the Ina River valley varied significantly, the flow also changed its dynamic parameters. Consequently, large boulders were deposited first, forming the core of the future boulder bars. The boulder sizes, determined from both satellite images and field surveys, range widely, reaching 9–10 m and, in one case, up to 32 m. These dimensions are similar to, and in some cases exceed, those of boulders transported during the Yigong outburst flood (Wu et al., 2020).

Boulder Bars 1 and 2 were formed in the immediate vicinity of Ina Dam I as a result of its failure and are composed primarily of large boulder material. Boulders 3-5m (or less) in diameter are clearly visible on the bar surface. A series of low terraces (4-6 m, 8-10 m, and 10-15 m in height) are located in the area between Bar 2 and Bar 3. The first major widening of the Ina River valley is the mouth of the Akul River (Fig. 2), where boulder bar 3 and 4, of considerable width and length (up to 3 km in total), have formed. A decrease in flow velocity led to the deposition of coarse-grained sediments. Downstream, a 10-15 m high terrace dominates this section. The next wide section of the valley is located at the confluence of the Turokcha and Ina rivers (Fig. 2). At the river's entrance to the valley widening zone, a series of terraces with a maximum height of 50 m are present (Fig. 3a, profile AB). On the upper terrace, the height of the gravel suggests a minimum flow depth exceeding that in this section. Here, there is a thin layer of sediment overlying the bedrock. Particularly noteworthy is bar 5, composed of poorly stratified sediments up to 30 m high. It has a classic crescent shape, formed in the lee of a bedrock spur (Fig. 3a).

Bar 6 occupies a wide section of the valley (Fig. 5a) and has a thin layer of boulder deposits, the sections of which are most clearly visible in the frontal part. Because the bar surface is eroded in some places by paleochannels (most likely associated with the final part of the breach), a unique depositional landscape of ridges, hills and spillways has formed (Fig. 4a and b). Isolated erratic boulders and blocks are found on the surface of the main part of bar 6 (Fig. 4c). Analyzing the profile across the Ina River valley suggests that the frontal part of bar 6 (left bank) and the 60-m-high deposits (right bank) may have once been a single unit (Fig. 5a, profile EF). However, given that the flow depth reached 50 m and its dynamics were significantly reduced, the origin of the boulders at a height of 60 m remains unclear. It is possible that these deposits belong to an earlier, unknown outburst flood event or are relict glacial deposits from before the LGM.

Also noteworthy are the 40-45 m terrace deposits adjacent to the 60 m boulders. Their sequence begins with channel pebbles overlying the bedrock (Fig. 5c). Higher in the section are colluvial deposits and then horizontally stratified sands. The upper part of the section, formed under subaerial conditions, is represented by eolian sands and buried soils. As the section shows, some of the deposits (pebbles) formed in the riverbed under conditions similar to the present. Subsequently, deep erosional incision into the bedrock occurred, removing these pebble deposits from the influence of the active channel. The change in the erosional base and incision into the bedrock could have been associated with the uplift of a block (the Ikatskii Ridge) bounded by the Ukshum Fault or with the subsidence of the Barguzin Basin during normal fault movements along the Barguzin Fault (Chipizubov et al., 2007). Notably, the amplitude of normal fault movements along the Barguzin Fault (~8-9 m) is comparable to the amplitude of incision into the bedrock (~8 m). Following this incision, colluvium began to accumulate on the surface of the gravel.

Terrace deposits, 15-20 m and 10-15 m thick and composed of sand and gravel (slackwater deposits), were formed over a short period (Figs. 6b and 12). They probably resulted from the rapid settling of particles from highly concentrated suspensions during a period of declining flow velocity. The source of this volume of sand and gravel deposits may have been saprolite, formed by the weathering of granite bedrock that is widespread in the area. It is also possible that the landslide-dammed Upper Ina paleolake, which existed for some time, was an area where sandy-gravel sediments accumulated. These sediments were subsequently eroded and transported to the lower part of the valley.

Regarding the genetic relationship between deposits within bars, alluvial fans and landslide debris, the most significant criterion for correlating them is their common bedrock composition. Granites, which make up the Ina Dam I and Ina Dam II deposits, are widespread throughout the study area. These same rocks predominate in the structure of bars 5, 6, and the IRG. This indicates a common source for the debris: the granite massifs. The morphology of the debris reflects differences in the dynamics and duration of transport. The landslide deposits are characterized by angular debris, indicating short-term gravitational movement without significant mechanical processing. In contrast, the bars and IRG deposits are dominated by coarsely rounded debris, a result of their transport and reworking in the riverbed. IRG deposits are characterized by high variability in both boulder morphology and size. A clear relationship between the degree of roundness and clast size is observed: as the grain size decreases, the intensity of mechanical processing increases. Localized clusters of boulders with minimal mechanical wear on their surfaces are also recorded, for example, in the upper part of the Outburst fan boulder field I. Their formation is likely related to nearby bedrock sources, suggesting extremely limited transport, both in distance and duration. The similarity of bedrock confirms a common source for the landslide deposits, bars, and the fan. Boulder morphology serves as an indicator of the transport mode: from short-term gravitational movement (landslides) to prolonged fluvial transport (bars, alluvial fan). The presence of both rounded and fresh, angular rock fragments in the fluvial deposits indicates complex sedimentation dynamics, associated with the episodic input of new material from the slopes into the catastrophic flow.

Thus, the study of bars, terraces and fluvial deposits in the Ina Valley

has made it possible to identify three main lithofacies. These correspond to successive hydrodynamic phases of the transit and waning of a catastrophic flood flow. The first group is represented by accumulations of coarse clastic material, including poorly rounded and angular boulders, as well as giant blocks ranging in size from the first meters to 9-10 m across. These formations are spatially confined to the alluvial fan at the mouth of the Ina River and are also found as isolated erratic blocks on the surface of high terraces and bars. Morphologically, the clasts are characterized by an angular or sub-angular shape with uneven, fractured faces and a complete absence of features indicative of long-distance fluvial transport. The lithology of the blocks is identical to the bedrock composing the valley walls in areas of landsliding and the breach site, which unambiguously points to a local source and an extremely limited transport distance. A distinctive feature of the blocks is their exceptionally weak degree of post-depositional alteration: their upper surfaces are unaffected by chemical weathering processes, and desert varnish, weathering rinds, and macroscopically visible fracturing are absent. This fact indicates the geological youth of the deposits and their exposure over a short time interval, which is consistent with the Holocene age for the event. The second group of deposits constitutes a poorly sorted, massive (non-stratified) sequence composed of pebble-gravel material with an abundant sand-silt matrix. Large boulders and isometric blocks are randomly distributed within the sequence, showing no oriented fabrics, cross-bedding, or graded bedding. The absence of sedimentary structures and selective deposition is interpreted as the result of a catastrophic dumping of bedload and suspended sediments during a sharp decrease in the transport capacity of the flow. The high concentration of debris (boulders, pebbles, gravel and sand) and the increased viscosity of the fluid suppressed turbulent structures, resulting in rapid en masse deposition. The third group (slackwater deposits) is composed mainly of sands, completing the section of the flood alluvium. This facies corresponds to the final stage of flood attenuation, marking the transition of the flow to a lower regime. The sands, sometimes with an admixture of fine gravel, are characterized by distinct horizontal or gently undulating lamination, resulting from the migration of small bedforms and the settling of suspended sediment from turbulent suspension during a sharp decrease in velocity and depth. The thickness of the sand lenses varies depending on the hypsometric position: maximum values are recorded on the surface of floodplain terraces, where the most complete deposition of fine-grained suspension occurred. The vertical and lateral succession of the described lithotypes within the Ina River valley demonstrates a classic model of sedimentation during catastrophic outburst floods.

4.3. Maximum discharge of the Ina outburst flood

The obtained numerical values for maximum discharge vary from 3.9×10^4 m^3/s to 13.2×10^4 m^3/s. Thus, the extreme values of maximum discharge differ by more than a factor of three, which introduces significant uncertainty into the assessment of the flow energy. In this context, it is useful to consider historical events with similar parameters. One such event is the Yigong outburst flood (Zhu et al., 2003; Shang et al., 2003; Delaney and Evans, 2015; Liu et al., 2019; Turzewski et al., 2019 Wu et al., 2020). The outburst flood occurred on June 10, 2000, on the Yigong River, a tributary of the Yarlung Tsangpo. Two months earlier, a landslide with a volume of $109 + 6$ Mm^3 dammed the Yigong River, forming a landslide-dammed lake with a maximum volume of 2.015 Gm^3 (Delaney and Evans, 2015). These volume parameters for the Yigong landslide and landslide-dammed Yigong Lake are quite close to the parameters of Ina Dam I (100 Mm^3) and the landslide-dammed Upper Ina paleolake (2.17 Gm^3). The maximum discharge for the Yigong outburst flood according to Delaney and Evans (2015), was 61,461 m^3/s. Other estimates of the maximum discharge, probably calculated near the Tongmai Bridge, are 126,400 m^3/s (Zhu et al., 2003). Shang et al. (2003) also reported a maximum instantaneous discharge of approximately 120,000 m^3/s at the Tongmai Bridge, 17 km downstream from the dam. Thus, available maximum discharge data for the Yigong outburst flood also show considerable variation. Taking into account our own maximum discharge parameters for the Ina outburst flood (Table 4), we can assume a comparable range of approximately 64, 000 m^3/s to 131,916 m^3/s.

The maximum elevation of alluvium recorded near Bar 5 suggests a minimum water depth of 50 m at this location. Downstream, at a distance of 7.2 km and an elevation of 26 m, boulders and gravel-pebble deposits associated with the Ina outburst flood are found. This indicates that the flow depth at the outlet from the mountain valley into the depression was greater than 26 m. The cross-sectional area of the valley near Bar 5 is 15,000 m^2. Accordingly, the flow velocity will be 4.2 m/s and 8.8 m/s at the extreme values of maximum discharge. The cross-sectional area of the valley near the mouth of the Ina River at the outlet from the mountain valley into the depression is 6625 m^2. Accordingly, applying the extreme discharge values yields flow velocities of 9.6 m/s and 19.9 m/s, respectively. Unfortunately, the true peak discharge parameters at any point in the valley remain unknown without dedicated modeling studies. However, we can estimate flow velocities for the onset of sediment erosion using the flow depth and the size of the largest sediment transported at the mouth of the valley. Since the IRG contains boulders measuring 9-10 m in diameter, we can use this parameter in our calculations.

A more direct assessment of transport capacity was performed using an empirical hydraulic formula of Shamov (1954) linking flow velocity (V), depth (h), and the diameter (d) of entrained sediment: $V = 4.4\, d^{0.33} h^{0.16}$. For a 10-m boulder (d) and a 26-m flow depth (h) at the valley mouth, the critical velocity for initiating motion is calculated to be 15.74 m/s. This value aligns well with the maximum simulated velocity of 14.57 m/s for the Yigong flood (Delaney and Evans, 2015). Using this critical velocity (15.74 m/s) and the valley mouth cross-sectional area (6625 m^2), the implied peak discharge would be ~104,277 m^3/s, a value within the mid-to-upper range of our independent estimates.

However, significant uncertainties must be acknowledged. The primary uncertainty concerns the wide range of peak discharge estimates, which directly influences flow velocity calculations. While useful as a first-order estimate, the applied empirical formula considerably simplifies the complex hydrodynamics of the flow and the processes of particle entrainment. Modeling results of the Yigong River outburst flood (Turzewski et al., 2019) compellingly demonstrate that such catastrophic events generate anomalously high and sustained bed shear stresses. A key characteristic is not only their expected concentration within morphological constrictions of the valley, but also the formation of an extensive zone of extreme boundary stress immediately downstream of the landslide dam breach. According to the modeling data (Turzewski et al., 2019), during the initial phase, within the first ~17 km of the inundation zone, shear stresses reached or exceeded the 5 kPa threshold. One hour after breach initiation, peak shear stress values persisted along the first 40 km, while simultaneously becoming localized at specific sites where sharp flow concentration occurred within valley constrictions. The steep segment of the Po River channel within the Tsangpo Gorge represents the most illustrative example of the destructive potential of such events. Here, modeled shear stresses ranged between 5 and 20 kPa. This stress level is sufficient to entrain and transport boulders up to 1 m in size (at 10% exposure) and even blocks up to 5 m in size (at 20% exposure) over an extended period—exceeding 9 h of the active flood phase.

These modeling results are directly corroborated by field investigations of the sedimentology and stratigraphy of the Yigong outburst flood deposits (Wu et al., 2020). Bar surface surveys indicate

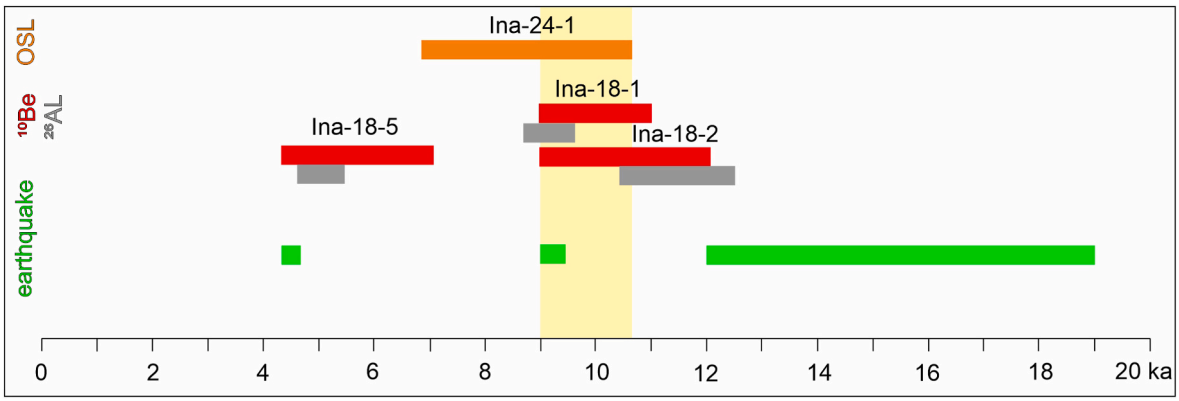

Fig. 13. Distribution of ^{10}Be-^{26}Al exposure ages of the outburst flood boulders (red, grey rectangle), OSL dates (orange rectangle) and the timing of paleoearthquakes (green rectangle) along the Barguzin Fault.

that the maximum recorded clast axis on boulder bars reached 5.08 × 20.93 m. Such extreme clast dimensions strongly suggest that the vast majority of boulders on the surface of these depositional landforms were not simply reworked, but were detached from their source and transported by the Yigong flood event (Wu et al., 2020). Morphometric analysis of boulder surfaces in both the Yigong and the Ina River valleys reveals an important transport characteristic: the overwhelming majority of transported clasts exhibit sub-angular (poorly rounded) forms. This observation directly indicates minimal abrasion during transport. The preservation of angular outlines unambiguously points to a relatively short transport distance for these clasts.

Regarding the dimensions of the "Ship" boulder (32 × 12 × 2.5 m), its transport likely required localized hydraulic conditions beyond the scope of this basin-scale analysis and warrants separate, future investigation. Nevertheless, despite uncertainties inherent in the hydraulic reconstruction, the calculated flow velocities support the hypothesis that the Ina outburst flood possessed sufficient energy to transport the mega-boulders deposited at the IRG. This conclusion is supported by the velocities' calibration against grain-size-based critical velocity thresholds, along with supporting modeling results and analyses of sediment morphology and facies variations from the Yigong River landslide dam outburst flood (Turzewski et al., 2019; Wu et al., 2020).

4.4. Age of the Ina outburst flood

To determine the age of the Ina outburst flood, we collected and dated samples from features related to the flood event. A series of dates (^{26}Al, ^{10}Be) were obtained from IRG boulders, and one OSL date was obtained from sediments on a 15-m terrace. Among the cosmogenic isotope dates, the most consistent are samples Ina-18-1 and Ina-18-2, which yielded ^{10}Be ages of 9.96 ± 1 ka and 10.54 ± 1.58 ka, and ^{26}Al of 9.12 ± 0.4 ka and 11.4 ± 1.13 ka, respectively. OSL dating produced ages of 8.7 ± 2.0 ka for quartz and 12 ± 4 ka for feldspar, which fall within the range defined by the cosmogenic isotope dates. If the dam failure was triggered by earthquake shaking, the Barguzin and Ukshum faults, both of which exhibit seismogenic deformations, are the most likely sources. In both cases, the estimated shaking intensity ranges from 8.5 to 9.5, depending on the magnitude and depth of the hypocenter.

The activation time for the Ukshum Fault is unknown. For the Barguzin Fault, however, data on the recurrence of strong earthquakes are available (Chipizubov et al., 2007). Based on seismogeological data, it has been determined that large earthquakes occurred on the southwestern segment of the Barguzin fault during the periods of 19-12 ka, 9.1-9.4 ka, and 4.5 ka (Chipizubov et al., 2007; Arzhannikova, 2021). Thus, there is a correlation between an earthquake in the Barguzin fault zone and the failure of the dam in the Ina River valley (Fig. 13). The formation of the dammed lake probably occurred earlier, between 19 and 12 ka. Nevertheless, the influence of the Ukshum Fault cannot be ruled out due to its proximity to the landslides and its high seismic potential. In Fig. 13, the colored, bold lines on the timeline represent the incertainty bands for the ^{10}Be, ^{26}Al and OSL data and the activation periods of the Barguzin Fault. These data constrain the probable time of the Ina outburst flood to between 9.1 ka and 10.7 ka.

Consequently, geochronological studies have enabled a precise constraint on the timing of the Ina outburst flood. These studies employed cosmogenic (^{10}Be, ^{26}Al) surface exposure dating of boulders on the fan and OSL dating of sandy sediments from the 15-m terrace. The integrated analysis of these dates provides new data that significantly refine the chronology of the Ina outburst flood beyond previous estimates (e.g., Ufimtsev et al., 2004). Based on a detailed analysis of regional paleoseismicity and original field data from the Ina River Valley, we conclude that strong paleoearthquakes were the trigger for large-scale landsliding. The seismogenic sources for these events are associated with the Barguzin and Ukshum fault zones. This seismic activity initiated a cascade of catastrophic processes: initial ground shaking induced slope failures that blocked the river valley, creating landslide-dammed lakes. The eventual breach of these unstable dams, likely triggered by subsequent earthquakes, generated a high-energy outburst flood. This catastrophic flow profoundly altered the valley's morphology. Our data thus establish a direct causal chain linking regional tectonics, slope instability, and a major outburst flood in the Ina River Valley.

5. Conclusion

In this study, we investigated the formation of landslide-dammed lakes and their subsequent catastrophic drainage down the Ina River valley within the Baikal Rift Zone. We propose that landslide-damming of the Ina River valley may have been caused by seismicity associated with movements on the Barguzin and Ukshum fault zones, which have seismic potential of M ~7.5–8.0 and M ~7, respectively. Repeated paleoearthquakes could have caused the destruction of landslides and the formation of the Ina outburst flood. Abrupt lake drainage and high-energy floodwaters up to 50 m deep produced an array of bars, terraces, bedrock remnants, narrow canyons, spillways, paleochannels, and the transport of boulders including the formation of a large boulder fan several kilometers long. We describe such fluvial forms here in detail.

Erosion and deposition associated with the Ina outburst flood are distributed unevenly throughout the Ina River valley. Based on the observed fluvial geomorphology of Ina Dam I and the landslide-dammed Upper Ina paleolake, we estimated water depth, flow velocity, and peak instantaneous discharge. Flow dynamics varied depending on the shape and size of the valley, resulting in a sharp differentiation in sediment size. The width and length of boulder bars are proportional to valley

width, and their height varies with distance from the dam.

Cosmogenic ^{10}Be, ^{26}Al and OSL dating yielded an age for the Ina outburst flood between 9.1 and 10.7 ka. This interval matches the estimated timing (9.1 – 9.4 ka) of a paleoearthquake linked to the Barguzin fault zone, although we cannot rule out the possibility of a coseismogenic link to the nearby Ukshum Fault.

CRediT authorship contribution statement

S.G. Arzhannikov: Writing – original draft, Visualization, Methodology, Investigation, Conceptualization. **A.V. Arzhannikova:** Writing – review & editing, Investigation, Conceptualization. **R. Braucher:** Writing – review & editing, Methodology, Data curation. **A.A. Chebotarev:** Investigation.

Declaration of competing interest

The authors declare that they have no known competing financial interests or personal relationships that could have appeared to influence the work reported in this paper.

Acknowledgments

We thank ASTER Team (G. Aumaître, K.Keddadouche) for their help measuring ^{10}Be, ^{26}Al. ASTER AMS, national facility (CEREGE, Aix en Provence), is supported by the INSU/CNRS and IRD and member of AIX MARSEILLE PLATFORMS and REGEF networks. Remote sensing analysis was possible thanks to the TanDEM-X project DEM_GEOL1188. The work was carried out using the equipment of the Center for Collective Use "Geodynamics and Geochronology" of the Institute of the Earth's crust SB RAS. We also express our gratitude to Alena Yakhnenko and Vladimir Vasiliev for their assistance in conducting field research. Many thanks to three anonymous reviewers for their valuable comments and advices.

References

Adams, J., 1981. Earthquake-dammed lakes in New Zealand. Geology 9, 215–219.

Alho, P., Russell, A.J., Carrivick, J.L., Käyhkö, J., 2005. Reconstruction of the largest Holocene jökulhlaup within Jökulsá á Fjöllum, NE Iceland. Quat. Sci. Rev. 2319–2334.

Arnold, M., Merchel, S., Bourlès, D.L., Braucher, R., Benedetti, L., Finkel, R.C., Aumaître, G., Gottdang, A., Klein, M., 2010. The French accelerator mass spectrometry facility ASTER: improved performance and developments. Nuclear Instruments and methods in physics research section B: Beam Interactions with Materials and Atoms 268, 1954–1959. https://doi.org/10.1016/j.nimb.2010.02.107.

Arzhannikov, S.G., 1998. Seismotectonics of the Sayano-Tuva Upland: Abstract of Dissertation of Candidate of Geological Sciences, Irkutsk, p. 17 in Russian.

Arzhannikov, S.G., 2000. Paleoseismodislocations in the Ottugtaigino-Azassky fault zone (Eastern Tuva). Geol. Geophys. 41 (11), 1499–1509 in Russian.

Arzhannikov, S.G., Alekseev, S.V., Glyzin, A.V., Kulagina, N.V., Ignatova, N.V., Orlova, L. A., 2010. The late Pleistocene-Holocene climate history in the western Todzha Basin (Eastern Tuva). Geol. Geophys. 51 (2), 206–221 in Russian.

Arzhannikov, S.G., Ivanov, A.V., Arzhannikova, A.V., Demonterova, E.I., Jansen, J.D., Preusser, F., Kamenetsky, V.S., Kamenetsky, M.B., 2018. Catastrophic events in the Quaternary outflow history of Lake Baikal. Earth Sci. Rev. 177, 76–113. https://doi.org/10.1016/j.earscirev.2017.11.011.

Arzhannikov, S., Arzhannikova, A., Braucher, R., Komatsu, G., 2023. Darhad megaflood (southern Siberia): cause, age and consequence. Quat. Int. 643, 1–21. https://doi.org/10.1016/j.quaint.2022.10.002.

Arzhannikova, A.V., 2021. Morphostructural evolution of Pribaikalia and Transbaikalia in the Late Mesozoic-Cenozoic. Dissertation abstract for the degree of Doctor of Geological and Mineralogical Sciences. Irkutsk, 32 pp. (in Russian).

Arzhannikova, A.V., Arzhannikov, S.G., Tetenkin, A.V., Chebotarev, A.A., Timofeeva, I. V., Efremova, U.S., Gladkochub, E.A., Bryanskiy, N.V., 2025. Chronology of glacial megafloods in the Baikal-Patom Upland (South Siberia): new geochronological constraints. Quat. Int. 749 (110004). https://doi.org/10.1016/j.quaint.2025.110004.

Baker, V.R., 2009. Overview of megaflooding: earth and Mars. In: Burr, D.M., Carling, P. A., Baker, V.R. (Eds.), Megaflooding on Earth and Mars. Cambridge University Press, Cambridge, UK, pp. 1–12. https://doi.org/10.1017/CBO9780511635632.

Baker, V.R., 2020. Global megaflood paleohydrology. In: Herget, J., Fontana, A. (Eds.), Palaeohydrology: Traces, Tracks and Trails of Extreme Events. Springer International Publishing, Cham, pp. 3–28. https://doi.org/10.1007/9.

Batbaatar, J., Gillespie, A.R., 2016a. Outburst floods of the Maly Yenisei. Part I. Int. Geol. Rev. 14, 1723–1752. https://doi.org/10.1080/00206814.2015.1114908.

Batbaatar, J., Gillespie, A.R., 2016b. Outburst floods of the Maly Yenisei. Part II - new age constraints from Darhad basin. Int. Geol. Rev. 14, 1753–1779. https://doi.org/10.1080/00206814.2016.1193452.

Benitoa, G., Thorndycraft, V.R., 2020. Catastrophic glacial-lake outburst flooding of the patagonian Ice Sheet. Earth Sci. Rev. 200 (102996). https://doi.org/10.1016/j.earscirev.2019.102996.

Bjornstad, B.N., 2021. Ice age floodscapes of the Pacific Northwest. A Photographic Exploration, Springer. https://doi.org/10.1007/978-3-030-53043-3, 180 pp.

Borchers, B., Marrero, S., Balco, G., Caffee, M., Goehring, B., Lifton, N., Nishiizumi, K., Phillips, F., Schaefer, J., Stone, J., 2016. Geological calibration of spallation production rates in the CRONUS-earth project. Quat. Geochronol. 31, 188–198. https://doi.org/10.1016/j.quageo.2015.01.009.

Braucher, R., Merchel, S., Borgomano, J., Bourles, D.L., 2011. Production of cosmogenic radionuclides at great depth: a multi element approach. Earth Planet Sci. Lett. 309. https://doi.org/10.1016/j.epsl.2011.06.036.

Braucher, R., Guillou, V., Bourlès, D.L., Arnold, M., Aumaître, G., Keddadouche, K., Nottoli, E., 2015. Preparation of ASTER in-house ^{10}Be/^{9}Be standard solutions. Nucl. Instrum. Methods Phys. Res. Sect. B Beam Interact. Mater. Atoms 361. https://doi.org/10.1016/j.nimb.2015.06.012.

Breckenridge, A., 2015. The Tintah-campbell gap and implications for glacial Lake Agassiz drainage during the younger dryas cold interval. Quat. Sci. Rev. 117, 124–134. https://doi.org/10.1016/j.quascirev.2015.04.009.

Bretz, J.H., 1928. The channeled scabland of eastern Washington. Geogr. Rev. 18, 446–477.

Bretz, J.H., Smith, H.T.U., Neff, G.E., 1956. Channeled Scabland of Washington: new data and interpretations. Geol. Soc. Am. Bull. 67, 957–1049.

Brown, E.T., Edmond, J.M., Raisbeck, G.M., Yiou, F., Kurz, M.D., Brook, E.J., 1991. Examination of surface exposure ages of Antarctic moraines using in situ produced 10Be and 26Al. Geochem. Cosmochim. Acta 55, 2269–2283. https://doi.org/10.1016/0016-7037(91)90103-C.

Carling, P.A., Kirkbride, A.D., Parnachov, S., Borodavko, P.S., Berger, G.W., 2002. Late Quaternary catastrophic flooding in the Altai Mountains of south-central Siberia: a synoptic overview and introduction to flood deposit sedimentology. In: Martini, I.P., Baker, V.R., Garzon, G. (Eds.), Flood and Megaflood Processes and Deposits: Recent and Ancient Examples, International Association of Sedimentologists Special Publication, 32. Blackwell Science, London, pp. 17–35. https://doi.org/10.1002/9781444304299.ch2.

Carling, P.A., 2013. Freshwater megaflood sedimentation: what can we learn about generic processes? Earth Sci. Rev. 125, 87–113. https://doi.org/10.1016/j.earscirev.2013.06.002.

Carozzi, M., Carozzi, A.V., 1987. Sulzer's antidiluvialist and catastrophist theories on the origins of mountains. Archives des Sciences. Genève 40, 107–143.

Carrivick, J., Tweed, F., 2019. A review of glacier outburst floods in Iceland and Greenland with a megafloods perspective. Earth Sci. Rev. 196 (102876). https://doi.org/10.1016/j.earscirev.2019.102876.

Carter, D.T., Ely, L.L., O'Connor, J.E., Fenton, C.R., 2006. Late Pleistocene outburst flooding from pluvial Lake Alvord into the Owyhee River, Oregon. Geomorphology 75, 346–367. https://doi.org/10.1016/j.geomorph.2005.07.023.

Chebotarev, A.A., Arzhannikov, S.G., Arzhannikova, A.V., Kurbanov, R.N., 2024. Origin of the badar sand field and the late Pleistocene tectonic movements in the tunka depression, the Baikal Rift Zone, Eastern Siberia. J. Asian Earth Sci. 260 (105957). https://doi.org/10.1016/j.jseaes.2023.105957.

Chen, J., Dai, F., Lv, T., Cui, Z., 2013. Holocene landslide-dammed lake deposits in the Upper Jinsha River, SE Tibetan Plateau and their ages. Quat. Int. 298, 107–113. https://doi.org/10.1016/j.quaint.2012.09.018.

Chen, N., 2014. The stability analysis of Xiao Lake barrier dam, Diexi. China Water Transport 14 (12), 180–181 (in Chinese with English abstract).

Chipizubov, A.V., Arzhannikov, S.G., Semyonov, R.M., Smekalin, O.P., 2007. Prehistoric earthquakes and fault scarps in the Barguzin fault zone. Geol. Geophys. 48 (7), 755–768.

Chmeleff, J., von Blanckenburg, F., Kossert, K., Jakob, D., 2010. Determination of the 10Be half-life by multicollector ICP-MS and liquid scintillation counting. Nucl. Instrum. Methods Phys. Res. Sect. B Beam Interact. Mater. Atoms 268, 192–199. https://doi.org/10.1016/j.nimb.2009.09.012.

Clayton, J.A., Knox, J.C., 2008. Catastrophic flooding from Glacial Lake Wisconsin. Geomorphology 93, 384–397. https://doi.org/10.1016/j.geomorph.2007.03.006.

Clarke, G.K.C., Leverington, D.W., Teller, J.T., Dyke, A.S., 2004. Paleohydraulics of the last outburst flood from glacial Lake Agassiz and the 8200 BP cold event. Quat. Sci. Rev. 23, 389–407. https://doi.org/10.1016/j.quascirev.2003.06.004.

Costa, J.E., 1985. Floods from dam failures. Open-File Rep. No. 85–560. U.S. Geological Survey, Denver.

Costa, J.E., Schuster, R.L., 1987. The formation and failure of natural dams. Open-File rep. No. 87–392. U.S. Geol. Survey, Vancouver, Washington.

Cui, P., Han, Y.S., Chen, X.Q., 2009. Distribution and risk analysis of dammed lakes reducedby Wenchuan earthquake. J. Sichuan Univ. (Eng. Sci. Ed.) 41 (3), 35–42 (in Chinese with English abstract).

Delaney, K.B., Evans, S.G., 2015. The 2000 Yigong landslide (Tibetan Plateau), rockslide-dammed lake and outburst flood: review, remote sensing analysis, and process modelling. Geomorphology 246, 377–393. https://doi.org/10.1016/j.geomorph.2015.06.020.

Evans, S.G., 1986. The maximum discharge of outburst floods caused by the breaching of man-made and natural dams. Can. Geotech. J. 23 (3), 385–387. https://doi.org/10.1139/t86-053.

Evans, S.G., Delaney, K.B., Hermanns, R.L., Strom, A.L., Scarascia-Mugnozza, G., 2011. The formation and behaviour of natural and artificial rockslide dams; implications for engineering performance and hazard management. In: Evans, S.G., et al. (Eds.), Natural and Artificial Rockslide Dams. Lecture Notes in the Earth Sciences, 133. Springer, Heidelburg, pp. 1–75. https://doi.org/10.1007/978-3-642-04764-0.

Fan, X., van Westen, C.J., Korup, O., Görüm, T., Xu, Q., Dai, F., Huang, R., Wang, G., 2012a. Transient water and sediment storage of the decaying landslide dams induced by the 2008 Wenchuan earthquake, China. Geomorphology 171–172, 58–68.

Fan, X., van Westen, C.J., Xu, Q., Gorum, T., Dai, F., 2012b. Analysis of landslide dams induced by the 2008 Wenchuan earthquake. J. Asian Earth Sci. 57, 25–37. https://doi.org/10.1016/j.jseaes.2012.06.002.

Farr, T.G., Rosen, P.A., Caro, E., Crippen, R., Duren, R., Hensley, S., Kobrick, M., Paller, M., Rodriguez, E., Roth, L., Seal, D., Shaffer, S., Shimada, J., Umland, J., Werner, M., Oskin, M., Burbank, D., Alsdorf, D., 2007. The shuttle radar topography mission,. Rev. Geophys. 45, RG2004. https://doi.org/10.1029/2005rg000183.

Fisher, T.G., 2020. Megaflooding associated with glacial Lake Agassiz. Earth Sci. Rev. 201 (102974). https://doi.org/10.1016/j.earscirev.2019.102974.

Florensov, N.A., 1960. Mesozoic and Cenozoic depressions of pribaikalia. Moscow-Leningrad, Izd. USSR Acad. Sci. 258 in Russian.

Galbraith, R.F., Roberts, R.G., Laslett, G.M., Yoshida, H., Olley, J.M., 1999. Optical dating of single grains of quartz from Jinmium rock shelter, northern Australia. Part I: experimental design and statistical models. Archaeometry 41, 339–364.

Gilbert, G.K., 1890. Lake Bonneville: U.S. Geological Survey Monograph 1, 438 P.

Gosse, J.C., Phillips, F.M., 2001. Terrestrial in situ cosmogenic nuclides: theory and application. Quat. Sci. Rev. 20, 1475–1560. https://doi.org/10.1016/S0277-3791(00)00171-2.

Gusev, V.N., Shobogorov, P.Ch, 1979. Geologic Map of the USSR, M 1:200000. Series Pribaikalskaya, Explanatory Note. N-49-XXI, Moscow, 1979, 98 pp. (in Russian).

Hassan, A.I., 2022. Cenozoic sedimentary deposits in the Barguzin and Tunka valleys of the Baikal rift system. Thesis PhD Geol. Sci. Irkutsk, 205 (in Russian).

Høgaas, F., Longva, O., 2016. Mega deposits and erosive features related to the glacial lake Nedre Glomsjø outburst flood, southeastern Norway. Quat. Sci. Rev. 151, 273–291. https://doi.org/10.1016/j.quascirev.2016.09.015.

Hu, H.-P., Feng, J.-l., Chen, F., 2018. Sedimentary records of a palaeo-lake in the middle Yarlung Tsangpo: implications for terrace genesis and outburst flooding. Quat. Sci. Rev. 192, 135–148. https://doi.org/10.1016/j.quascirev.2018.05.037.

Huang, S.-Y., Chen, Y.-G., Burr, G.S., Jaiswal, M.K., Lin, Y.-N., Yin, G.-M., Liu, J.-W., Zhao, S.-J., Cao, Z.-Q., 2014. Late Pleistocene sedimentary history of multiple glacially dammed lake episodes along the Yarlung-Tsangpo river, southeast Tibet. Quat. Res. 82, 430–440. https://doi.org/10.1016/j.yqres.2014.06.001.

Huang, X., Zhang, Y., Guo, Y., Ge, Y., Mao, P., Liu, T., Wang, S., 2024. Outburst flood events since the last glacial maximum in the Hutiao gorge of Jinsha River: geomorphological evidence from eddy gravel bars. Geomorphology 465 (109415). https://doi.org/10.1016/j.geomorph.2024.109415.

Jansen, R.B., 1980. Dams and Public Safety: Denver, Colorado, U.S. Department of the Interior, Bureau of Reclamation. Colorado, Denver, p. 332.

Jolivet, M., Ritz, J.-F., Vassallo, R., Larroque, C., Braucher, R., Todbileg, M., Chauvet, A., Sue, C., Arnaud, N., De Vicente, R., Arzhanikova, A., Arzhanikov, S., 2007. Mongolian summits: an uplifted, flat, old but still preserved erosion surface. Geology 35 (10), 871–874.

Kaktins, U., Davis Todd, C., Wojno, S., Coleman, N.M., 2013. Revisitingthe timing and events leading to and causing the Johnstown flood of 1889. Penn. Hist.: A J. Mid-Atlantic Stud. 80 (3), 335–363. https://doi.org/10.5325/pennhistory.80.3.0335.

Komatsu, G., Arzhannikov, S.G., Gillespie, A., et al., 2009. Quaternary paleolake formation and cataclysmic flooding along the upper Yenisei River. Geomorphology 104, 3–4. https://doi.org/10.1016/j.geomorph.2008.08.009, 143–164.

Komatsu, G., Baker, V., Arzhannikov, S., 2016. Catastrophic flooding, palaeolakes, and late Quaternary drainage reorganization in northern Eurasia. Int. Geol. Rev. 58 (14), 1693–1722. https://doi.org/10.1080/00206814.2015.1048314.

Korschinek, G., Bergmaier, A., Faestermann, T., Gerstmann, U.C., Knie, K., Rugel, G., Wallner, A., Dillmann, I., Dollinger, G., von Gostomski, ChL., Kossert, K., Maiti, M., Poutivtsev, M., Remmert, A., 2010. A new value for the half-life of 10Be by Heavy-ion elastic recoil detection and liquid scintillation counting. Nuclear instruments and methods in physics research section B: Beam Interactions with Materials and Atoms 268, 187–191. https://doi.org/10.1016/j.nimb.2009.09.020.

Lamakin, V.V., 1952. Ushkanyi Islands and the Problem of Baikal Formation. Moscow, 199 pp. (in Russian).

Lamakin, V.V., 1968. Neotectonics of the Baikal Basin. Nauka, Moscow, 247.

Lang, J., Alho, P., Kasvi, E., Goseberg, N., Winsemann, J., 2019. 2019. Impact of middle Pleistocene (Saalian) glacial lake-outburst floods on the meltwater-drainage pathways in northern central Europe: insights from 2D numerical flood simulation. Quat. Sci. Rev. 209, 82–99. https://doi.org/10.1016/j.quascirev.2019.02.01.

Liu, W., Carling, P., Hu, K., Wang, H., Zhou, Z., Zhou, L., Liu, D., Lai, Z., Zhang, X., 2019. Outburst floods in China: a review. Earth Sci. Rev. 197 (102895), 10/1016/j.earscirev.2019.102895.

Logatchev, N.A., 2003. History and geodynamics of the Baikal rift. Russ. Geol. Geophys. 44 (5), 373–387.

Logatchev, N.A., Zorin, Y.A., 1987. Evidence and causes of the 2-stage development of the Baikal rift. Tectonophysics 143 (1-3), 225–234.

Lunina, O.V., Gladkov, A.S., 2007. Late Cenocoic fault pattern and stress fields in the Barguzin Rift. Geol. Geophys. 48 (7), 775–789 in Russian.

Maizels, J.K., 1997. Jökulhlaup deposits in proglacial areas. Quat. Sci. Rev. 16, 793–819.

Margold, M., Jansen, J., Codilean, A., Preusser, F., Gurinov, A., Fujioka, T., Fink, D., 2018. Repeated megafloods from lake Vitim, Siberia, to the arctic jcean over the past 60000 years. Quat. Sci. Rev. 187, 41–61. https://doi.org/10.1016/j.quascirev.2018.03.005.

Mats, V.D., Ufimtsev, G.F., Mandelbaum, M.M., Alakshin, A.M., Pospeev, A.V., Shimaraev, M.N., Khlystov, O.M., 2001. The Baikal Basin in the Cenozoic: Structure and Geologic History. Siberian Branch of RAS Publishing House, Filial "Geo", Novosibirsk, p. 252 (in Russian).

McCalpin, J.P., 1996. Paleoseismology. Academic Press, San Diego, p. 585.

Meinsen, J., Winsemann, J., Weitkamp, A., Landmeyer, N., Lenz, A., Dölling, M., 2011. Middle Pleistocene (Saalian) lake outburst floods in the Münsterland Embayment (NW Germany): impacts and magnitudes. Quat. Sci. Rev. 30, 2597–2625. https://doi.org/10.1016/j.quascirev.2011.05.014.

Merchel, S., Bremser, W., 2004. First international 26Al interlaboratory comparison - part I. Nucl. Instrum. Methods Phys. Res. Sect. B Beam Interact. Mater. Atoms 223–224, 393–400. https://doi.org/10.1016/j.nimb.2004.04.076.

Merchel, S., Arnold, M., Aumaître, G., Benedetti, L., Bourlès, D.L., Braucher, R., Alfimov, V., Freeman, S.P.H.T., Steier, P., Wallner, A., 2008. Towards more precise 10Be and 36Cl data from measurements at the 10-14 level: influence of sample preparation. Nucl. Instrum. Methods Phys. Res. Sect. B Beam Interact. Mater. Atoms 266, 4921–4926. https://doi.org/10.1016/j.nimb.2008.07.031.

Montgomery, D.R., Hallet, B., Liu, Y.-P., Finnegan, N., Anders, A., Gillespie, A., Greenberg, H.M., 2004. Evidence for Holocene megafloods down the Tsangpo River gorge, southeastern Tibet. Quat. Res. 62, 201–207. https://doi.org/10.1016/j.yqres.2004.06.008.

Murray, A., Arnold, L.J., Buylaert, J.-P., Guerin, G., Qin, J., Singhvi, A.K., Smedley, R., Thomsen, K.J., 2021. Optically stimulated luminescence dating using quartz. Nat. Rev. Methods Primers 1, 72.

O'Connor, J.E., 1993. Hydrology, hydraulics, and geomorphology of the Bonneville flood. Geol. Soc. Am. Spec. Pap. 274 (83). https://doi.org/10.1130/SPE274-p1.

O'Connor, J.E., Clague, J.J., Walder, J.S., Manville, V., Beebee, R.A., 2022. 6.36-Outburst floods. In: Shroder, J.F. (Ed.), Treatise on Geomorphology. Academic Press, San Diego, pp. 765–819. https://doi.org/10.1016/B978-0-12-818234-5.00007-9.

Panizzo, A., Girolamo, P., Risio, M., Maistri, A., Petaccia, A., 2005. Great landslide events in Italian artificial reservoirs. Nat. Hazards Earth Syst. Sci. 5, 733–740. https://doi.org/10.5194/nhess-5-733-2005.

Pardee, J.T., 1910. The glacial Lake Missoula. J. Geol. 18, 376–386.

Pardee, J.T., 1942. Unusual currents in glacial Lake Missoula, Montana. Geol. Soc. Am. Bull. 53, 1569–1599.

Petit, C., Déverchère, Jacques, 2006. Structure and evolution of the Baikal rift: a synthesis. Geochem. Geophys. Geosyst, 7, Q11016. https://doi.org/10.1029/2006GC001265.

Ravskii, E.J., Alexandrova, L.P., Vangeigem, E.A., Gerbova, V.G., Golubeva, L.V., 1964. Anthropogene Deposits of Southern East Siberia. Nauka, Moscow, p. 215 in Russian.

Ravskii, E.I., 1972. Sedimentation and Climates of Inner Asia in the Anthropogene. Nauka, Moscow, 336.

Rudoy, A.N., Baker, V.R., 1993. Sedimentary effects of cataclysmic late Pleistocene glacial outburst flooding, Altay Mountains, Siberia. Sediment. Geol. 85, 53–62. https://doi.org/10.1016/0037-0738(93)90075-G.

Russell, A.J., Fay, H., Marren, P.M., Tweed, F.S., Knudsen, Ó., 2005. Icelandic jökulhlaup impacts. In: Caseldine, C.J., Russell, A.J., Knudsen, Ó., Harðardóttir, H. (Eds.), Iceland: Modern Processes and past Environments. Developments in Quaternary Science, 5, pp. 154–203, 10.1016/S1571-0866(05)80009-0.

Shamov, G.I., 1954. River Sediments. Gidrometeoizdat, Leningrad, 347.

Shang, Y., Yang, Z., Li, L., Liu, D., Liao, Q., Wang, Y., 2003. A super-large landslide in Tibet in 2000: background, occurrence, disaster, and origin. Geomorphology 54, 225–243.

Shebalin, N.V., 1968. Methods of using engineering-seismological data in seismic zoning. In: Solonenko, V.P. (Ed.), Seismic Zoning of the USSR. M. Nauka, pp. 95–111 in Russian.

Skovitina, T.M., 1996. Earthquakes as triggers for development of dam-lakes in rift basins of the Baikal Rift system, East Siberia, EOS, Transactions. AGU 77 (46), 511–512.

Skovitina, T.M., 2002. The barrier lakes of the Sayan-Baikal mountain region. Geomorfologiya 3, 79–88 in Russian.

Solonenko, V.P., 1962. Determination of epicentral zones of earthquakes based on geological features. Bulletin of the USSR Academy of Sciences. Geological Series 11, 58–74.

Stone, J.O., 2000. Air pressure and cosmogenic isotope production. J. Geophys. Res. 105, 753–759. https://doi.org/10.1029/2000JB900181.

Strom, A., Abdrakhmatov, K., 2018. Rockslides and Rock Avalanches of Central Asia: Distribution, Morphology, and Internal Strukture. Elsevier, p. 449.

Turzewski, M.D., Huntington, K.W., LeVeque, R.J., 2019. The geomorphic impact of outburst floods: integrating observations and numerical simulations of the 2000 Yigong flood, eastern Himalaya. Journal of Geophysical research: Earth Surf. 124, 1056–1079. https://doi.org/10.1029/2018JF004778.

Ufimtsev, G.F., 1986. Traces of a giant ejection of rocky material from the Ina River valley into the Barguzin Basin. Geogr. Nat. Resour. 3, 73–78 in Russian.

Ufimtsev, G.F., Skovitina, T.M., Kulchitsky, A.A., 1998. Rockfall-Dammed Lakes in the baikal region: evidence from the past and prospects for the future. Nat. Hazards 18 (2), 167–183.

Ufimtsev, G.F., Skovitina, T.M., Rezanov, I.N., 2004. Insky Garden of Stones. - Irkutsk: Izd-Vo Institute of Geography SB RAS, 39 P (in Russian).

Waitt, R.B., 2016. Megafloods and Clovis cache at Wenatchee, Washington. Quat. Res. 85, 430–444. https://doi.org/10.1016/j.yqres.2016.02.007.

Wang, Y.R., Wang, Z.Y., 2005. The "75•8" Catastrophic Flood Disaster in Henan Province. Yellow River Water Conservancy Press, China, p. 305 (in Chinese).

Wells, D.L., Coppersmith, K.J., 1994. New empirical relationships among magnitude, rupture length, rupture area, and surface displacement. Bull. Seismol. Soc. Am. 84, 974–1002. https://doi.org/10.1785/BSSA0840040974.

Wiedmer, M., Montgomery, D., Gillespie, A., Greenberg, H., 2010. Late Quaternary megafloods from Glacial Lake atna, Southcentral Alaska. USA. Quat. Res. 73, 413–424. https://doi.org/10.1016/j.yqres.2010.02.005.

Wu, C., Hu, K., Liu, W., Wang, H., Hu, X., Zhang, X., 2020. Morpho-sedimentary and stratigraphic characteristics of the 2000 Yigong River landslide dam outburst flood deposits, eastern Tibetan Plateau. Geomorphology 367 (107293). https://doi.org/10.1016/j.geomorph.2020.107293.

Xu, C., Xu, X., Zheng, W., 2013. Compiling inventory of landslides triggered by Minxian-Zhangxian earthquake of July 22, 2013 and their spatial distribution analysis. J. Eng. Geol. 21 (5), 736–749.

Zhang, J.Y., Yang, Z.H., Jiang, J.P., 2014. A Study on Reservoir Dam Defects and Breaches in China. Science Press, Beijing, China, p. 290 (in Chinese).

Zhu, P.Y., Wang, C.H., Wang, Y.C., 2003. Large-scale landslide-debris avalanche in Tibet, China. Formation of an exceptionally serious outburst flood from a landslide dam in Tibet. Landslide News 14–15, 23–25.

Zolnikov, I.D., Deev, E.V., 2013. Quaternary glacial superfloods at the Gorny Altai: formation conditions and geological features. Earths Cryosphere 4, 74–82. In Russian.